Blast furnace slag-based alkali-activated concrete with treated municipal solid waste incineration (MSWI) bottom ash as coarse aggregate

Mechanical properties, freeze-thaw resistance, and environmental impact

Chen, Boyu; Paul, Ivana Mariam; Miranda de Lima, Luiz; Holthuizen, Patrick; He, Shan; Aytekin, Burcu; Zeng, Yu; Ye, Guang

DOI
10.1016/j.jobe.2025.115015

Publication date
2025

Document Version
Final published version

Published in
Journal of Building Engineering

Citation (APA)
Chen, B., Paul, I. M., Miranda de Lima, L., Holthuizen, P., He, S., Aytekin, B., Zeng, Y., & Ye, G. (2025). Blast furnace slag-based alkali-activated concrete with treated municipal solid waste incineration (MSWI) bottom ash as coarse aggregate: Mechanical properties, freeze-thaw resistance, and environmental impact. *Journal of Building Engineering*, *118*, Article 115015. https://doi.org/10.1016/j.jobe.2025.115015

Journal of Building Engineering 118 (2026) 115015

Contents lists available at ScienceDirect

Journal of Building Engineering

journal homepage: www.elsevier.com/locate/jobe

Blast furnace slag-based alkali-activated concrete with treated municipal solid waste incineration (MSWI) bottom ash as coarse aggregate: Mechanical properties, freeze-thaw resistance, and environmental impact

Boyu Chen [a,1,*], Ivana Mariam Paul [a,1], Luiz Miranda de Lima [a], Patrick Holthuizen [a], Shan He [a], Burcu Aytekin [a], Yu Zeng [a], Guang Ye [a,b,**]

[a] Department of Materials and Environment (Microlab), Faculty of Civil Engineering and Geoscience, Delft University of Technology, Delft, the Netherlands

[b] Magnel-Vandepitte Laboratory, Department of Structural Engineering and Building Materials, Ghent University, 9052, Ghent, Belgium

ARTICLE INFO

Keywords:
MSWI bottom ash coarse aggregate
Alkali-activated concrete
Mechanical properties
Freeze-thaw resistance
Life cycle assessment

ABSTRACT

Municipal solid waste incineration (MSWI) bottom ash (BA) is widely available and has been increasingly explored for sustainable concrete production. While it is commonly used in Ordinary Portland Cement (OPC)-based concrete, its application in alkali-activated concrete (AAC) remains rare. This study developed a new AAC using MSWI BA as coarse aggregate to evaluate whether this represents a more sustainable application pathway compared to its use in conventional concrete. To address issues associated with metallic aluminum (Al) in MSWI BA, a NaOH-based pre-treatment was applied to reduce its content and minimize surface cracking and volume expansion in AAC. The incorporation of treated MSWI BA increased the overall porosity of AAC. The interfacial transition zone (ITZ) surrounding MSWI BA exhibited characteristic microstructural features. While previous studies suggested that MSWI BA-induced porosity may enhance freeze-thaw resistance in OPC concrete, the opposite trend was observed in AAC. The increased pore volume, irregular pore shapes, and MSWI BA-related microcracking reduced freeze-thaw durability. Despite these challenges, the developed AAC retained mechanical performance within strength class C30/37 and achieved a substantially lower carbon footprint compared to OPC and CEM III/B concretes. Leaching assessments further confirmed that the developed AAC complied with environmental standards and did not release harmful contaminants. Overall, these findings demonstrate that MSWI BA is a promising coarse aggregate for AAC.

* Corresponding author.
** Corresponding author. Department of Materials and Environment (Microlab), Faculty of Civil Engineering and Geoscience, Delft University of Technology, Delft, the Netherlands.
E-mail addresses: Chen_Boyu@hotmail.com (B. Chen), ivanamariampaul@gmail.com (I.M. Paul), l.mirandadelima@tudelft.nl (L. Miranda de Lima), p.e.holthuizen@tudelft.nl (P. Holthuizen), s.he-2@tudelft.nl (S. He), b.aytekinturkoglu@tudelft.nl (B. Aytekin), y.zeng-4@tudelft.nl (Y. Zeng), g.ye@tudelft.nl (G. Ye).
[1] Both authors contributed equally.

https://doi.org/10.1016/j.jobe.2025.115015
Received 22 July 2025; Received in revised form 1 December 2025; Accepted 15 December 2025
Available online 18 December 2025

1. Introduction

As the world's third most widely used material, concrete has a significant environmental impact due to its main components: Ordinary Portland Cement (OPC) and natural aggregates [1,2]. The production of OPC accounts for approximately 8 % of global anthropogenic carbon emissions [3]. The extensive extraction of natural aggregates disturbs ecological stability and accelerates environmental degradation [4]. In response to these challenges, research efforts have increasingly focused on identifying sustainable alternative materials that can either partially or fully replace OPC and natural aggregates.

The pursuit of environmentally sustainable alternatives to OPC has driven the extensive development of Alkali-activated materials (AAMs). AAMs can be divided into alkali-activated paste (also called alkali-activated binder), alkali-activated mortar, and alkali-activated concrete (AAC), based on the type of aggregate incorporated [5]. This classification highlights the versatility of AAM systems across different material scales and construction applications. Among the various alkali-activated binders, those derived from blast furnace slag are the most extensively studied and most widely applied, owing to their proven performance and industrial scalability [6]. Properly designed AAC not only reduces environmental impact but also enhances resistance to chemical attack and long-term deterioration compared to OPC-based concrete [7]. However, natural aggregates are still predominantly used in AAC production [8]. Exploring alternative aggregate sources is therefore a promising strategy to further reduce the environmental impact of AAC.

Municipal solid waste incineration (MSWI) bottom ash is a major by-product of waste-to-energy processes [9]. For example, In Europe, annual MSWI bottom ash production reaches approximately 20 million tons [10]. In China, it exceeds 13 million tons per year [11]. With the continued expansion of waste-to-energy incineration projects worldwide [12–15], the generation of MSWI bottom ash is expected to increase, presenting both a waste management challenge and an opportunity for its beneficial utilization. The application of MSWI bottom ash as aggregate offers an economically viable solution [16,17]. MSWI bottom ash has been recognized as a viable replacement for natural aggregates, with numerous studies demonstrating its feasibility in OPC-based concrete [5,18–26].

Despite being widely utilized as aggregate in OPC-based concrete, MSWI bottom ash is rarely applied in AAC [27]. Previous research has primarily focused on using the fine MSWI bottom ash as a substitute for fine natural aggregate in AAC [28–30]. Compared with the fine MSWI bottom ash, its coarse counterpart generally exhibits superior quality due to better grading, lower water absorption, and reduced heavy metal content. Its lower chloride and sulfate content minimizes durability concerns, making it a more stable aggregate option [16,31,32]. Moreover, the application of coarse MSWI bottom ash as aggregate is more viable for large-scale industrial use, requiring less pre-treatment than its utilization as a binder material [16]. Accordingly, this study investigates the use of coarse MSWI bottom ash as aggregate in AAC to address this research gap and assess its potential for sustainable concrete production.

The use of coarse MSWI bottom ash in concrete presents two main challenges. The first challenge is its metallic aluminum (Al) content, which is higher than that of the fine MSWI bottom ash. The presence of metallic Al in MSWI bottom ash can lead to volume expansion and cracking in concrete [33,34]. NaOH-based pre-treatment is often employed to reduce the metallic Al content of MSWI bottom ash before it is incorporated into AAMs. The treatment parameters need to be adjusted on a case-by-case basis to ensure optimal performance and compatibility with specific mix designs [5,35]. The second challenge is the high water absorption of coarse MSWI bottom ash. Although it absorbs less water than the fine MSWI bottom ash, its absorption remains significantly higher than that of natural coarse aggregates. This elevated absorption can adversely affect the workability and compressive strength of concrete incorporating bottom ash as a coarse aggregate [34]. The treatments proposed in previous studies to reduce the water absorption of MSWI bottom ash aggregates include thermal treatment for material densification, washing or alkaline washing to remove soluble salts and fine particles, accelerated carbonation to fill internal pores through $CaCO_3$ formation, and surface encapsulation to seal open porosity [20]. In addition, MSWI bottom ash aggregates exhibit a high water absorption characteristic similar to that of recycled concrete aggregates (RCA). Given this similarity, mitigation strategies commonly used for RCA, such as pre-soaking, adjusting the mixing water content, or incorporating superplasticizers, might be applicable for addressing the increased water demand of MSWI

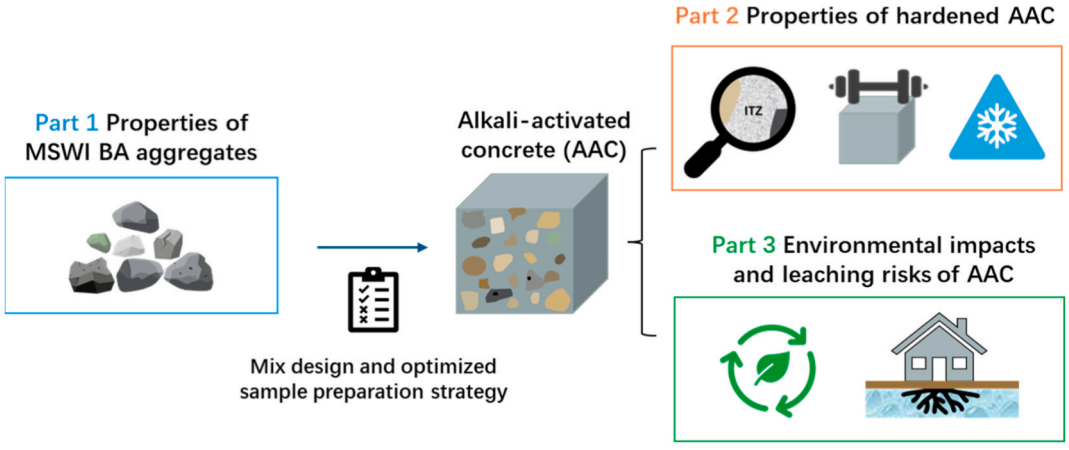

Fig. 1. The main content of this work.

bottom ash aggregates [36].

Coarse MSWI bottom ash has been reported to negatively affect the workability, strength, and volume stability of alkali-activated concrete. In contrast, several studies have shown that its incorporation can enhance the freeze-thaw resistance of OPC concrete. Lynn et al. [37] found that replacing 20 % of coarse aggregates with MSWI bottom ash in OPC concrete enhanced freeze-thaw resistance. This improvement was attributed to the ash acting as an air-entraining agent. However, the authors did not perform detailed microstructural analysis, such as interfacial transition zone (ITZ) examination or pore shape evaluation, to support this mechanism. Keulen et al. [17] reported that increasing the replacement level of MSWI bottom ash coarse aggregate to 100 % did not result in a significant mass loss in OPC-based zero-slump concrete exposed to freeze-thaw cycles. Notably, the potential benefits of using coarse MSWI bottom ash aggregates for improving freeze-thaw resistance have not been explored in AAC. Research on the freeze-thaw resistance of AAC is generally limited. The existing studies have reported conflicting results, with some suggesting that AAC performs similarly, better, or worse than OPC concrete under freeze-thaw conditions [28].

As discussed above, MSWI bottom ash has been rarely used as a coarse aggregate in AAC. Whether this represents a more sustainable utilization route than its use in conventional concrete remains to be determined. While MSWI bottom ash has been shown to improve freeze–thaw performance in OPC concrete, it is still unclear whether AAC, which often shows variable and sometimes poor freeze-thaw durability, can benefit in the same way. This study addresses this gap by evaluating the performance of AAC incorporating coarse MSWI bottom ash aggregate. As shown in Fig. 1, this work consists of three parts. Part 1 presents a detailed analysis of the physical properties of MSWI bottom ash aggregates, which forms the basis for the proposed pre-treatment method and concrete mix design. In part 2, the mechanical properties and freeze-thaw resistance of concrete containing bottom ash aggregates are evaluated, along with an analysis of the concrete microstructure. In part 3, a life cycle assessment (LCA) is conducted to systematically evaluate the environmental impact, and a comprehensive leaching assessment is performed to determine whether the material meets regulatory standards for environmental safety.

2. Materials and methods

2.1. Raw materials

The MSWI bottom ash (BA) aggregates used in this research are supplied by a Dutch company. As a commercial product, these MSWI BA aggregates are intended to replace 4–8 mm natural aggregates in Portland cement-based concrete. The image of this MSWI BA aggregate is shown in Fig. 2 (a). More detailed information regarding the chemical and mineralogical compositions of these aggregates can be found in our previous publication [38]. The production of these aggregates followed the same procedure proposed by Keulen et al. [17]. The treatment process mainly consists of dry separation, wet separation, and weathering (around 3 months). The dry separation is to extract both ferrous and non-ferrous metals, while the wet separation is to remove the organic and inorganic leachable contaminants. The purpose of weathering is to immobilize heavy metals and reduce the associated leaching risks. The heavy metal leaching of resultant MSWI BA aggregates complied with the open (granular) application criteria of the Dutch Soil Quality Decree [17].

The natural aggregates, consisting of river gravel and sand, were obtained from Sibelco Benelux B.V. (see Fig. 2(b)–(d)). The binder

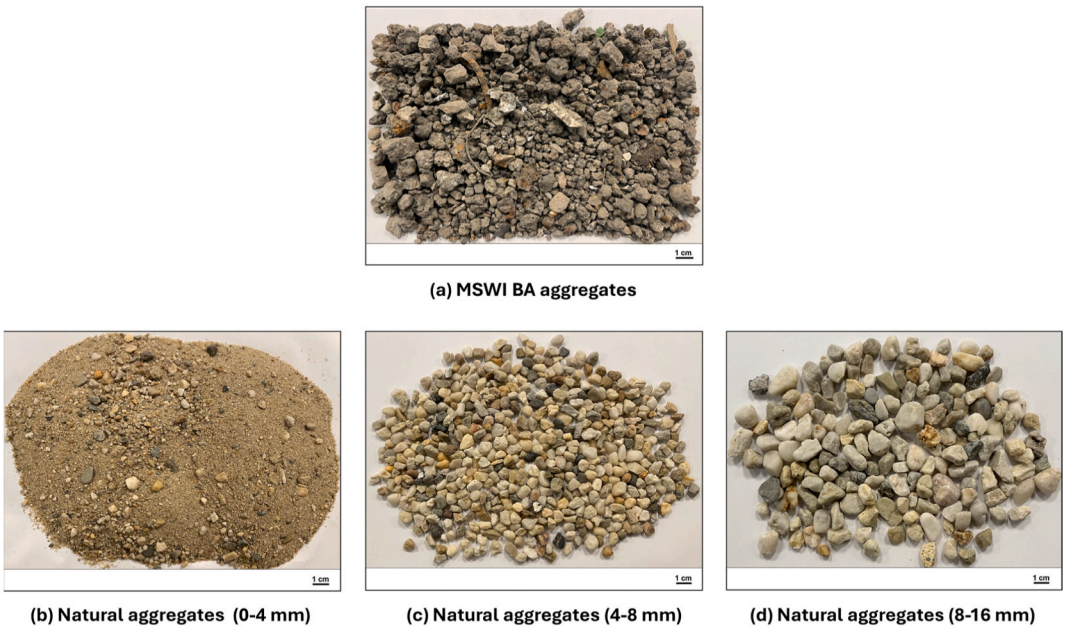

Fig. 2. MSWI BA aggregates and natural aggregates within the same size fraction.

of the alkali-activated concrete was prepared using ground granulated blast furnace slag (GGBFS) as single precursor. The GGBFS used in this research is the same as that used by Chen et al. [38]. The activator was prepared by mixing sodium hydroxide solution (50 % w/v) with water glass solution (modulus 2.0/2.1, 37.5 % w/v). The CEM III/B 42.5 N was used to prepare the reference concrete mix for comparison with the alkali-activated concrete.

2.2. Physical properties measurements for aggregates

The gradation of aggregates was determined by sieving analysis according to NEN-EN 933-1 [39]. The water absorption is a direct indicator of aggregate porosity and is calculated as the amount of water that the aggregates particles are capable of absorption. The water absorption test was conducted on oven-dried MSWI BA aggregates following NEN-EN 1097-6 [40]. Apparent particle density is defined as the ratio between the mass of aggregates that have been oven-dried and the volume they occupy when immersed in water. The loose bulk density is the weight of the aggregates contained in a defined volume, indicating the packing density. The test was conducted following the guidelines set by NEN-EN 1097-3 [41]. The Los Angeles (LA) coefficient indicates the resistance of the aggregates to abrasion under loading. The test was conducted in accordance with NEN-EN 1097-2 [42].

2.3. Concrete mix design

Zero-slump (earth-moist) concrete was selected as the target mixture because it corresponds directly to real industrial production processes for precast paving stones and curb units, which rely on very low water contents and high compaction pressure. In these systems, traditional workability concerns associated with MSWI bottom ash (e.g., increased water demand or slump loss) are irrelevant, as the consistency is governed by compaction rather than flowability [17]. Moreover, the inherent porosity of zero-slump mixtures helps dissipate any hydrogen gas generated from residual metallic Al, preventing matrix expansion or cracking [5]. Together, these factors make zero-slump concrete particularly suitable for high replacement levels of treated MSWI bottom ash in practice. Additionally, this mix design approach enhances the freeze-thaw resistance of AAC by reducing the amount of free water in the mix, which can otherwise cause internal damage during freezing cycles [43]. Since there is no established design provision for AAC, this study adopted a three-step mix design approach, which is explained below. The detailed mix design can be found in Table 1.

The **first step** was to design a reference mix in accordance with current standards, ensuring it meets the requirements for freeze-thaw resistance and slump. The selected parameters will serve as the baseline for designing alkali-activated concrete. Given that CEM III/B is the most widely used sustainable cement in the Netherlands, the first reference mixture is the CEM III/B concrete mix containing 100 % natural aggregates (hereafter denoted as 100NA-*BCC*). According to the NEN-EN 206 [44], concrete exposed to the XF4 environmental class must have a maximum water-to-cement ratio (w/c) of 0.45 and a minimum cement content of 340 kg/m^3. To ensure zero slump, the w/c ratio was set at 0.4, while the cement content was kept at the minimum specified content. Aggregate grading was determined based on the recommendations of NEN-EN 933-1 [45].

The **second step** focused on developing an alkali-activated reference concrete by modifying the mix design of the 100NA-BCC to achieve zero slump and a similar strength class. This alkali-activated reference concrete, also containing 100 % natural aggregates, is referred to as 100NA-*AAC*. The aggregate grading in 100NA-AAC was the same as that used in 100NA-BCC. The binder of 100NA-BCC was substituted with alkali-activated GGBFS. The activator was prepared by mixing NaOH solution, water glass solution, and water (see Table 1). Its composition was selected based on a series of preliminary trial-and-error mixes, in which compressive strength and slump were used as the main performance indicators. The activator contained 4.7 wt% Na_2O and 2.4 wt% SiO_2 relative to the precursor mass. The alkali modulus (SiO_2/Na_2O molar ratio) was 0.75. The water-to-solid ratio (w/s) was 0.43. The water content refers to the water present in the activator, while the solid content includes both the solid components of the activator and the precursor. The 100NA-AAC mix served as the reference for incorporating MSWI BA aggregates in AAC.

The **third step** was to partially replace the 4–8 mm natural aggregates in the 100NA-AAC mix with MSWI BA aggregates. As zero slump was required, workability was not a concern. Therefore, no extra water was added to compensate for the higher water absorption of the MSWI BA aggregates. Using the same activator dosage as in 100NA-AAC results in a lower effective water-to-binder (w/b) ratio in the bottom ash–incorporated AAC, which is expected to enhance compressive strength. In the end, 30 wt% of the 4–8 mm natural aggregates in the 100NA-AAC mix were replaced with MSWI BA aggregates. This replacement level was selected to meet the strength class C30/37, one of the most specified grades for structural concrete. The resulting mixture, containing 30 % bottom ash

Table 1
Mix designs for reference concrete and concrete containing MSWI BA aggregates.

Mixture	100NA-BCC	100NA-AAC	30BA-AAC	Unit
CEM III/B cement	340	–	–	kg/m^3
Ground granulated blast furnace slag	–	314	314	kg/m^3
Water glass solution (modulus 2.0/2.1, 62.5 wt% H_2O)	–	33.53	33.53	kg/m^3
NaOH solution (50 wt% NaOH in water)	–	25.15	25.15	kg/m^3
Water	136	109	109	kg/m^3
Natural aggregates (0–4 mm)	751	751	751	kg/m^3
Natural aggregates (4–8 mm)	557	557	390	kg/m^3
MSWI BA aggregates	–	–	167	kg/m^3
Natural aggregates (8–16 mm)	557	557	557	kg/m^3

coarse aggregates, is designated 30BA-*AAC*. It is important to note that when the replacement level of MSWI BA exceeds 30 %, the resulting alkali-activated concrete does not meet the required strength. This indicates that 30 % is the maximum allowable amount of MSWI BA under the current pre-treatment method. Furthermore, the alkaline solution used to treat the MSWI BA is drawn from the activator, following the same strategy used in our previous work [35]. When the MSWI BA replacement level exceeds 30 %, additional alkaline solution must be added, which results in an activator composition different from that used in 100NA-AAC.

2.4. Concrete sample preparation

2.4.1. Reference samples

In the preparation of 100NA-BCC, cement was first mixed with natural aggregates in a dry state for 4 min. Then, water was gradually added to this dry mixture. After mixing for 3 min, the fresh concrete was poured into molds for strength testing. Molds with dimensions of 150 × 150 × 150 mm were used for compressive and splitting tensile strength tests, while 400 × 100 × 100 mm molds were used for flexural strength tests. Since the fresh mixture exhibits zero slump, the molds were filled while applying vibration to ensure proper compaction and to eliminate air bubbles. The 100NA-AAC mix was prepared by following the same procedure as 100NA-BCC. Initially, GGBFS and natural aggregates were dry mixed, followed by the addition of the activator. Subsequently, the zero-slump fresh concrete mixture was cast into the molds, with vibration applied to ensure thorough compaction and the removal of air bubbles.

2.4.2. Samples containing MSWI BA aggregates

Unlike the reference concrete mixture, the 30BA-AAC mixture was prepared in a different way. The MSWI BA aggregates contain around 2 wt% of metallic Al. The metallic Al content was determined using the water displacement method. Details about this method can be found in our previous publications [33,46]. When using these bottom ash aggregates in alkali-activated concretes, volume expansion and cracking were observed due to the hydrogen (H_2) gas generated after the redox reaction of metallic Al. Therefore, the NaOH solution treatment was proposed in this work to reduce the metallic Al content in MSWI BA aggregates to below 1 wt%, as required by NEN-EN 12620 [47]. The selection of NaOH concentration, liquid-to-solid ratio, and curing duration was empirical and guided directly by the observed reduction in metallic Al content under different treatment conditions.

In this study, MSWI BA aggregates were pre-treated using 1 M NaOH at a liquid-to-solid mass ratio of 0.85, followed by sealed curing at room temperature for 14 days, which ensured sufficient reduction of metallic Al for use in AAC. To avoid the usage of extra amount of alkaline solution, the NaOH solution used for the treatment of MSWI BA aggregates was separated from the activator designated for the preparation of alkali-activated concrete [35]. In the end, the metallic Al content remaining in the treated MSWI BA aggregates is around 0.53 wt%. The treated MSWI BA aggregates were directly used for sample preparation and no cracks were observed on the surface of the early-age alkali-activated concrete containing MSWI BA aggregates.

As shown in Fig. 3, the preparation of 30BA-AAC was carried out in four steps. The mixing times were established through preliminary optimization using our laboratory equipment, as no universal standard exists and reported durations vary depending on the mixer type. The NaOH solution treatment of MSWI BA aggregates was included as Step 1 in the sample preparation procedure. In step 2, the treated MSWI BA aggregates were mixed with the remaining activator for 1 min. This activator was prepared by subtracting the NaOH solution that had been added during the pre-treatment process. In step 3, GGBFS was added and mixed thoroughly for 2–3 min. In step 4, the natural aggregates were incorporated and mixed for another 2 min to achieve a homogeneous mixture before casting. After casting, the 100NA-BCC, 100NA-AAC, and 30BA-AAC samples are sealed with a plastic film and stored in a curing room at 20 °C and 99 % relative humidity (RH) until the testing age.

2.5. Microstructure studies

The microstructural analysis of concrete focused on air voids in the binder matrix and MSWI BA aggregates, along with porosity and cracking in the interfacial transition zone (ITZ).

2.5.1. X-ray computed tomography (X-ray CT) analysis

X-ray CT analysis is a widely recognized non-destructive technique for examining the three-dimensional microstructure of materials. In this study, high-resolution X-ray CT scans with the TESCAN CoreTOM system were applied to analyze the air voids in concrete, specifically within the binder matrix and inside the MSWI BA aggregates. Cylindrical core specimens measuring 50 mm in diameter and 150 mm in height were extracted from 28-day cured concrete cubes to ensure representative sampling while maintaining scan quality. Prior to scanning, the specimens were dried for 24 h in a desiccator to remove surface moisture.

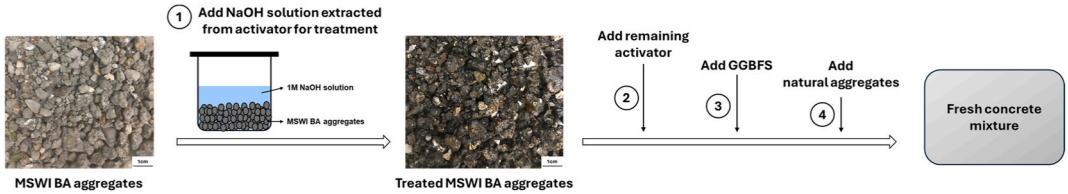

Fig. 3. The four-step procedure used to prepare AAC containing MSWI BA aggregates (30BA-AAC).

The CT scan was performed with a voltage of 140 kV and a power of 68 W. The test included both control samples (100NA-BCC and 100NA-AAC) and concrete samples containing MSWI BA aggregates (30BA-AAC). The sample was wrapped in plastic film and mounted on a rotating table for scanning (see Fig. 4). Each specimen was scanned in three sections, which were later merged to form a complete 3D reconstruction. The voxel size was 67.3 μm × 67.3 μm × 67.3 μm. The scans produced approximately 3000 projections. An example of CT projection for 30BA AAC is shown in Fig. 5, where the pores in MSWI BA aggregates are already distinctly visible. The CT projections were first reconstructed using Panthera software, after which the reconstructed CT slices were processed and analyzed using Dragonfly ORS software.

Due to the inevitable aggregate spalling during the sample collection process, additional pores may form at the sample surface and thus lead to overestimation of the porosity. Hence, a cylindrical zone, which is 40 mm in diameter and 100 mm in height, was selected as the region of interest (ROI) for further quantitative analyses (see Fig. 6). The Otsu method was applied to segment the pore phase, and the threshold was dynamically determined to include all the macropores [48]. An example of the segmentation process is shown in Fig. 6. It should be noted that some extremely fine cracks could be observed in BA-30 AAC, but they could not be accurately segmented due to the limited resolution. Therefore, only macropores were considered in further quantitative analyses. For this analysis, the pore size was defined with the minimum Feret diameter. The volume-weighted average sphericity ($\overline{S}_V$) was used as an index to assess pore shape. This index was calculated using the following formula: $\overline{S}_V = \frac{\sum(S_i \cdot V_i)}{\sum V_i}$, where S_i is the sphericity of an individual pore, V_i is the volume of the corresponding pore, and V_i is the total volume of all detected pores.

2.5.2. Scanning electron microscopy (SEM) analysis

SEM analysis was used to examine the morphology of MSWI BA aggregates in the concrete and their ITZ with the binder matrix. The 28-day concrete specimens were first cut using a diamond saw with water cooling and then dried to prevent microstructural alterations. To enhance stability, they were vacuum-impregnated with low-viscosity epoxy and cured for 24–48 h. The samples were sequentially ground using SiC papers (P180–P1200) under ethanol lubrication. After grinding, they were polished with diamond suspensions (6 μm, 3 μm, 1 μm) to achieve a smooth, reflective surface. The samples were then carbon-coated (~10–15 nm thick) to minimize charging effects during SEM imaging at 15 kV and a 10 mm working distance. The Energy Dispersive Spectroscopy (EDS) spot analysis was performed to differentiate MSWI BA aggregates from natural aggregates based on elemental composition and to identify slag particles in the binder matrix. This methodology ensured accurate microstructural characterization of the concrete components.

2.6. Performance evaluation of developed concrete

2.6.1. Mechanical testing

The mechanical properties of the developed concrete are evaluated in terms of compressive strength, tensile strength, and flexural strength to provide a comprehensive assessment. These data are crucial for determining the suitability of the concrete under different service conditions.

The compressive strength was assessed in accordance with the NEN-EN 12390-3 [49]. Measurements were obtained from three cube specimens at 1, 3, 7, and 28 days after casting, and the average strength was recorded.

The splitting tensile strength test, an indirect method for assessing the tensile strength of concrete, was conducted following NEN-EN 12390-6 [50]. Eight concrete cubes with dimensions of (150 × 150 × 150 mm) were tested, with hardboard packing strips applied to the loading surfaces. The mean tensile strength of the specimens was determined 28 days after casting.

Flexural strength measures the capacity of concrete to withstand these bending stresses. The flexural strength was measured through a 3-point bending test according to NEN-EN 14651 [51], using an INSTRON Universal Testing System with a 10 kN maximum load capacity. Concrete prisms with dimensions of (400 × 100 × 100 mm) were prepared, with a 2.5 mm notch added at the midpoint

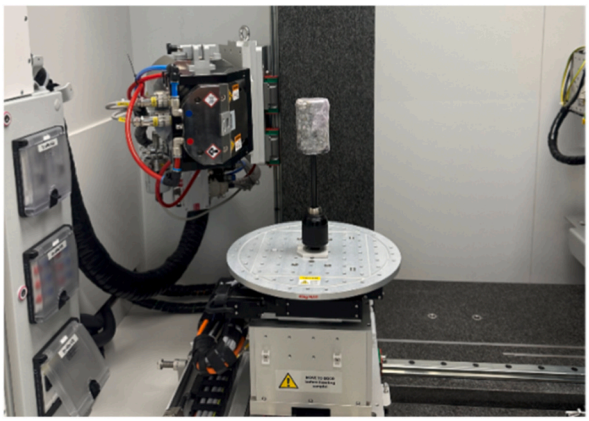

Fig. 4. Placement of the concrete specimen in the CT scanner.

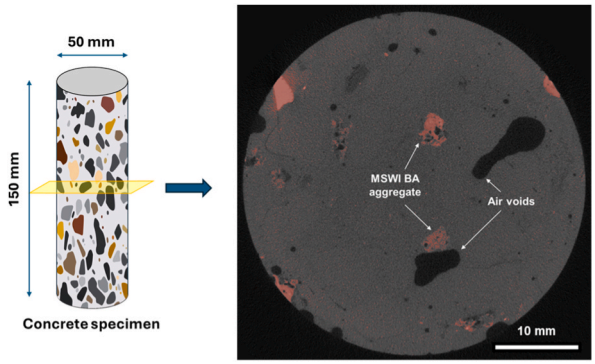

Fig. 5. An example of reconstructed CT slice from the 30BA-AAC specimen, in which porous MSWI bottom ash aggregates are visible and highlighted in red.

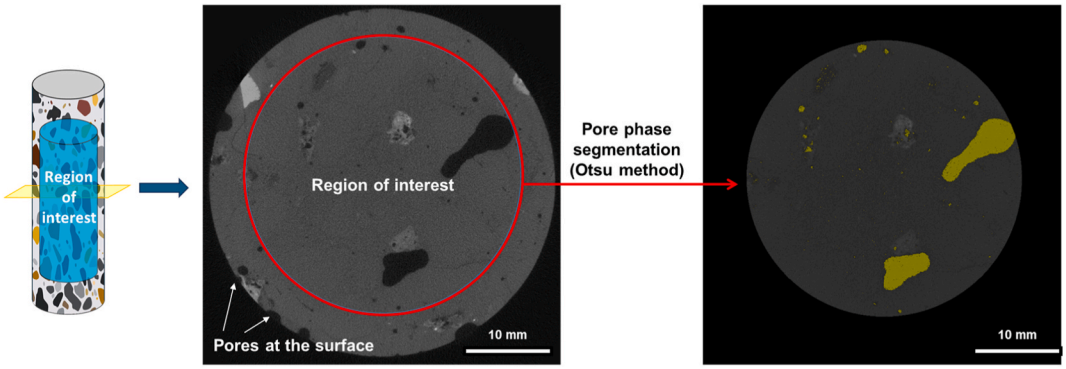

Fig. 6. Labeled region of interest (ROI) in the reconstructed CT slice from the 30BA-AAC specimen (left) and the processed image obtained after Otsu thresholding (right). The segmented air voids are highlighted in yellow.

along the width one day before testing. The test followed standard procedures, although the prism dimensions were slightly smaller than specified in the standard.

2.6.2. *Freeze-thaw resistance*

The freeze-thaw resistance of the concrete was assessed using the Capillary Suction of Deicing Chemicals and Freeze-Thaw (CDF) test method, following the guidelines of NVN-CEN/TS 12390-9 [52]. The evaluation involved measuring the extent of surface scaling on the sample. The specimens were cast in 150 mm × 150 mm × 150 mm molds, the same as those used for compressive strength testing. After 24 h, they were demolded, wrapped in plastic film, and placed in a curing room at 20 °C and 99 % relative humidity (RH) for 2 weeks. Following this curing period, the plastic film was removed, and the specimens were transferred to a controlled room set at 20 °C and 50 % RH for an additional 2 weeks.

The butyl tape was applied to the lateral surfaces to control exposure, leaving only the bottom surface uncovered. Before the freeze-thaw cycles, the concrete samples underwent a saturation phase, during which the exposed surface was placed facing downward and immersed in a 3 % NaCl solution for 7 days. The freeze-thaw cycles were initiated after saturation, with each cycle lasting 12 h and alternating between −20 °C and +20 °C. After each cycle, the containers were placed in an ultrasonic bath for 3 min to collect any scaled material. The 3 % NaCl solution used in the test was replenished after cycles 4, 6, 14, and 28. The collected material was dried at 110 ± 10 °C for 24 h and weighed after cooling to room temperature. The cumulative amount of scaled material per unit area (kg/m^2) after n cycles was calculated using the formula $S_n = \frac{m_{s,n}}{A} \cdot 10^3$, where S_n represents the mass of scaled material per unit area after the n-th cycle (kg/m^2), $m_{s,n}$ is the cumulative mass of dried scaled material after n freeze-thaw cycles, and A is the test surface area (mm^2). Three replicate samples were tested, and the average was calculated.

2.7. *Life cycle assessment (LCA)*

The primary objective of this LCA is to evaluate the environmental performance of AAC incorporating MSWI BA aggregates. Additionally, this study aims to identify the concrete ingredients that contribute most significantly to environmental impacts. The total shadow cost of AAC containing MSWI BA aggregates is also quantified to provide a comprehensive assessment of its economic and environmental viability.

The LCA follows the methodology outlined in ISO 14040 [53]. The functional unit is set to 1 m^3 of concrete with the same 28-day compressive strength. This approach allows for a fair assessment of their environmental impacts while maintaining consistency in performance evaluation. The AAC containing MSWI BA aggregates is compared to both alkali-activated concrete and conventional concrete sourced from the literature. It is important to note that only samples with the same strength class were considered in this analysis. Consequently, the number of mixtures from previous studies that meet this criterion is limited. The 28-day compressive strength and raw materials of these mixtures are detailed in Table 2. This table presents the amount of solids used to prepare the activator, specifically NaOH pellets and the solid content of water glass. It is worth noting that obtaining the life cycle inventory data for the same activator used in literature is challenging. In the LCA of the activator, only the solid components in the solution are considered, as water is assumed to have no environmental impact.

As specified in NEN-EN 15804 [54], every system—encompassing both products and processes—is categorized into four stages: the product stage, construction process stage, use stage, and end-of-life stage. Within the product stage, key processes include raw material supply (A1), transportation (A2), and manufacturing (A3). Given that this study focuses on comparing concrete systems with different raw material compositions, the emphasis is placed on raw material supply (A1) within the product stage. Additionally, for the concrete mixtures sourced from the literature, detailed LCA data on transportation and manufacturing processes are unavailable.

The life cycle inventory data for GGBFS, CEM I 42.5 N, and CEM III/B 42.5 N are sourced from the Environmental Product Declarations (EPDs) provided by their respective suppliers. Water, being a natural resource, is assumed to have no environmental impact. Data for NaOH pellets, water glass (100 % pure), sand, gravel, and limestone are obtained from the NIBE database [60]. Please refer to Table A 1, Table A 2, and Table A 3 for the life cycle inventory data of these raw materials.

The MSWI BA aggregates used in this study are derived from municipal solid waste incineration and are treated as secondary raw materials. In line with common LCA practice, they are considered free of environmental burden, as the associated impacts are attributed to the primary waste treatment process. This assumption is based on the system boundary approach, where the environmental burdens associated with the generation of MSWI BA are allocated to the primary waste treatment process (i.e., incineration of municipal solid waste) rather than the downstream applications utilizing the ash. Similar assumptions are widely adopted in LCA studies focused on circular economy and waste valorization contexts. Nonetheless, it is acknowledged that this simplification may not capture all potential environmental trade-offs.

The following assumptions were applied in the LCA analysis to ensure consistency across comparisons: (1) all gravel fractions were assumed to have equivalent environmental impacts, and (2) the raw materials used in literature-based mixtures were assumed to originate from the same suppliers as those used in the experimental concrete samples. The impact assessment evaluates 11 categories, as outlined in Table A 4. The total environmental impact (F_{total}) is determined using the equation $F_{total} = \Sigma F_i M_i$, where F_i represents the impact factor associated with a specific environmental indicator, and M_i denotes the mass of each constituent required to produce 1 m^3 of concrete. In the Netherlands, the Environmental Cost Indicator (ECI) is a standardized method used to quantify the total environmental impact of a product or process over its life cycle. The total ECI is calculated following the formula $ECI_{total} = \Sigma ECI_i M_i$, where ECI_i represents the shadow cost of raw material i (in €/kg or €/ton), and M_i is the mass of that material used in 1 m^3 of concrete. Based on the Stichting Bouwkwaliteit (SBK) methodology, the ECI evaluates environmental performance across 11 impact categories [61].

2.8. Leaching risks

Currently, there is no universally standardized leaching test specifically designed for construction materials. A comparative analysis of various international leaching protocols indicates that the Netherlands has established one of the most comprehensive and application-specific regulatory frameworks [62]. Given that the concrete in this study is intended for use in the Netherlands, the Dutch leaching test methods and regulatory criteria were selected for evaluation. The leaching analysis was conducted using a column leaching test in accordance with NEN 7375 [63]. The test was performed on 28-day-old concrete samples with dimensions of 100 × 100 × 100 mm^3, which were crushed to a particle size of less than 4 mm prior to testing. The experiment evaluated leaching behavior as a function of the liquid-to-solid (L/S) ratio through the percolation of the concrete sample. The cumulative leaching emissions were

Table 2
Concrete mixtures from the literature used in the LCA. The amount in kg presented is used prepare 1 m^3 concrete.

Name	Compressive strength (MPa)	GGBFS	CEM I 42.5 N	CEM III/B 42.5 N	NaOH pellets	Water glass (100 % pure)	Sand	Gravel	Crushed limestone	MSWI BA aggregate
AAC I [55]	46.75	400	–	–	22.4	37.044	650	1208	–	–
AAC II [56]	45.79	400	–	–	29.41	57.27	858	–	858	–
AAC III [56]	46.98	400	–	–	16.92	68.82	858	–	858	–
OPC I [57]	46	–	641	–	–	–	547	1013	–	–
OPC II [58]	46.5	–	400	–	–	–	665	1107	–	–
BCC I [59]	38.92[a]	–	–	350	–	–	792	1018	–	–

[a] Although the compressive strength of this mixture is slightly lower than the others, it still meets the strength class of C30/37.

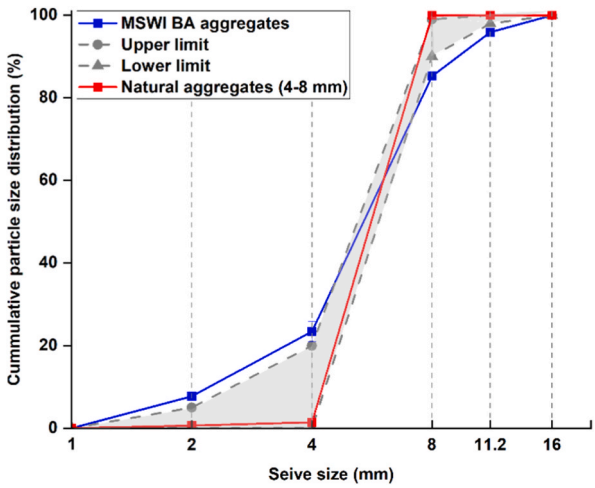

Fig. 7. Grading curves of MSWI BA aggregates and natural aggregates, alongside the lower and upper limit prescribed in the standard for the aggregates within the 4–8 mm size fraction.

quantified at an L/S ratio of 10 L/kg, with the leachate collected as a single cumulative eluate fraction. The leachate samples were characterized using inductively coupled plasma atomic emission spectroscopy (ICP-AES) to determine elemental concentrations. Additionally, ion chromatography (IC) was used to quantify chloride (Cl^-), bromide (Br^-), and sulfate (SO_4^{2-}), while fluoride (F^-) concentrations were measured using flow injection analysis with spectroscopic detection.

3. Results and discussion

3.1. Physical properties of MSWI BA aggregates

The physical properties of aggregates significantly influence the fresh and hardened properties of concretes. Properly graded aggregates contribute to optimal packing and manageable consistency in concrete, while enhancing its strength and durability. The grading curves of MSWI BA aggregates and natural aggregates were presented in Fig. 7. As can be seen in this figure, the grading curve of natural aggregates is within the shaded area defined by the upper and lower limits in NEN-EN 12620 [64]. Compared with natural aggregates, MSWI BA aggregates contain a higher proportion of fine particles. The grading of MSWI BA aggregates shows slight deviation compared to the norm limits for the 4–8 mm aggregates. Although some variation is observed, the grading still falls within the 15 % tolerance of the producer's declared values, as defined in NEN-EN 12620 [64]. This indicates that MSWI BA aggregate is a viable alternative to natural aggregate.

The water absorption, apparent density, loose bulk density, and the Los Angeles (LA) coefficient were measured to gain essential insights into the performance characteristics of MSWI BA aggregates and natural aggregates (see Table 3). Compared with natural aggregates, MSWI BA aggregates exhibit higher water absorption, lower density, and poorer abrasion resistance. These disadvantages of MSWI BA aggregates are primarily attributed to their higher porosity compared to natural aggregates [17]. The water absorption of MSWI BA aggregates is 7.04 wt%, which is ten times that of 4–8 mm natural aggregates (0.7 wt%). The high water absorption of MSWI BA aggregates increases the water demand in concrete mixtures when replacing natural aggregates. As a result, this can affect workability and influence the reaction of the precursor. The apparent density of MSWI BA aggregates is 2370 kg/m^3, and their loose bulk density is 1260 kg/m^3. The substitution of natural aggregates with MSWI BA aggregates with lower loose bulk density is likely to reduce packing density, resulting in increased porosity within the concrete and affecting its overall density and strength. Additionally, the LA coefficient of MSWI BA aggregates was 35.3, exceeding that of natural aggregates, indicating poorer resistance to mechanical wear and fragmentation. This reduced abrasion resistance suggests that MSWI BA aggregates are more prone to degradation under loading and impact.

Table 3
Physical properties of MSWI BA aggregates and natural aggregates.

Properties	MSWI BA aggregates	Natural aggregates		
		0–4 mm	4–8 mm	8–16 mm
Water absorption (wt.%)	7.04	0.10	0.70	0.57
Apparent density (kg/m^3)	2370	2640	2590	2610
Loose bulk density (kg/m^3)	1260	1750	1580	1540
Los Angeles coefficient	35.3	–	21.9	25

3.2. Properties of hardened AAC incorporating MSWI BA aggregates

3.2.1. Microstructure

The microstructure of the developed concrete was analyzed in terms of pore structure and the interfacial transition zone due to their significant influence on the mechanical properties and freeze-thaw resistance of concrete. The pore structure of concrete was analyzed in terms of pore characteristics (porosity, size distribution) and pore morphology (shape, partial filling).

3.2.1.1. Pore structure. Fig. 8 shows the reconstructed three-dimensional pore structure of 28-day concrete samples obtained from CT scanning. These detected pores mainly originate from air voids in the binder matrix and MSWI BA aggregates. The maximum pore size

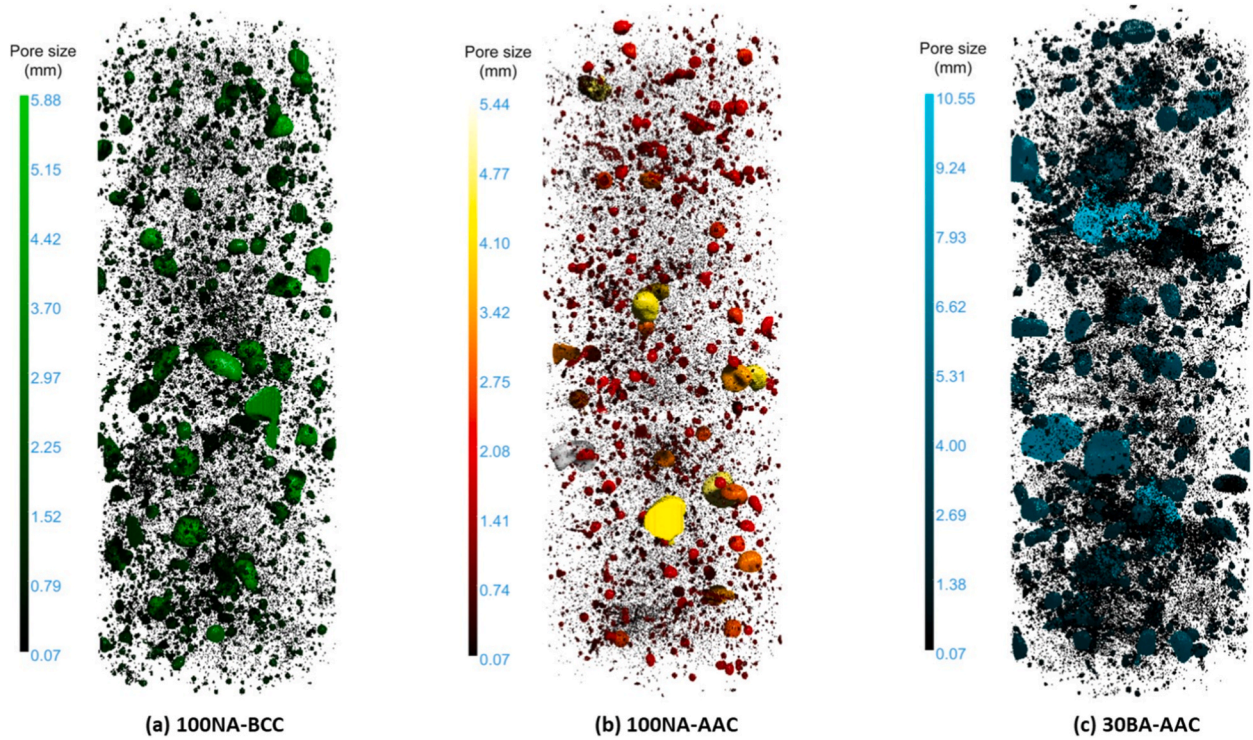

Fig. 8. Reconstructed three-dimensional pore structures of 28-day concrete samples: (a) 100NA-BCC; (b) 100NA-AAC; (c) 30BA-AAC. The pores are color-coded to distinguish different sizes.

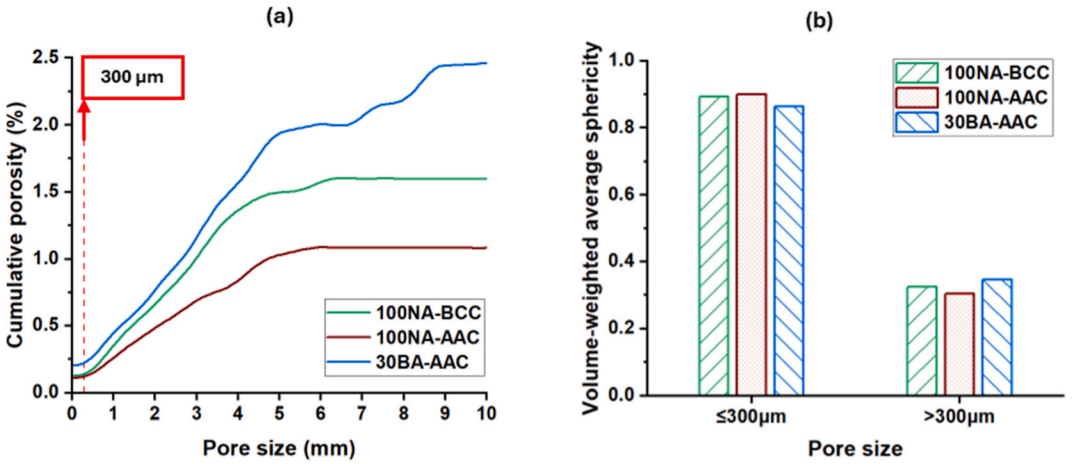

Fig. 9. (a) Cumulative volume and (b) Volume-weighted average sphericity ($\overline{S}_V$) of the pores in concrete samples, calculated based on their pore structure shown in Fig. 8.

in 30BA-AAC is significantly larger than that in two reference samples. The 30BA-AAC sample exhibits a more heterogeneous matrix with a higher concentration of large pores, whereas the 100NA-AAC sample presents a denser microstructure with fewer large pores. The pores shown in Fig. 8 were further analyzed in terms of their total volume sphericity, and morphology.

Fig. 9 (a) illustrates the cumulative porosity of the concrete samples. Among the three samples, 30BA-AAC exhibits the highest total porosity (2.54 %), while 100NA-AAC has the lowest (1.06 %), and 100NA-BCC falls in between (1.56 %). The porosity of concrete is primarily influenced by the binder type and aggregate properties. Blast furnace slag-based alkali-activated binders typically exhibit lower porosity compared to cement-based binders [65], which explains the higher porosity of 100NA-BCC relative to 100NA-AAC. When natural aggregates are replaced with MSWI bottom ash aggregates, additional pores are introduced. These pores originate from two sources: the intrinsic porosity of the bottom ash aggregates and the voids formed by the release of hydrogen gas during the oxidation of metallic Al present in the bottom ash.

The volume-weighted average sphericity describes the overall shape regularity of pores, with larger pores having a greater

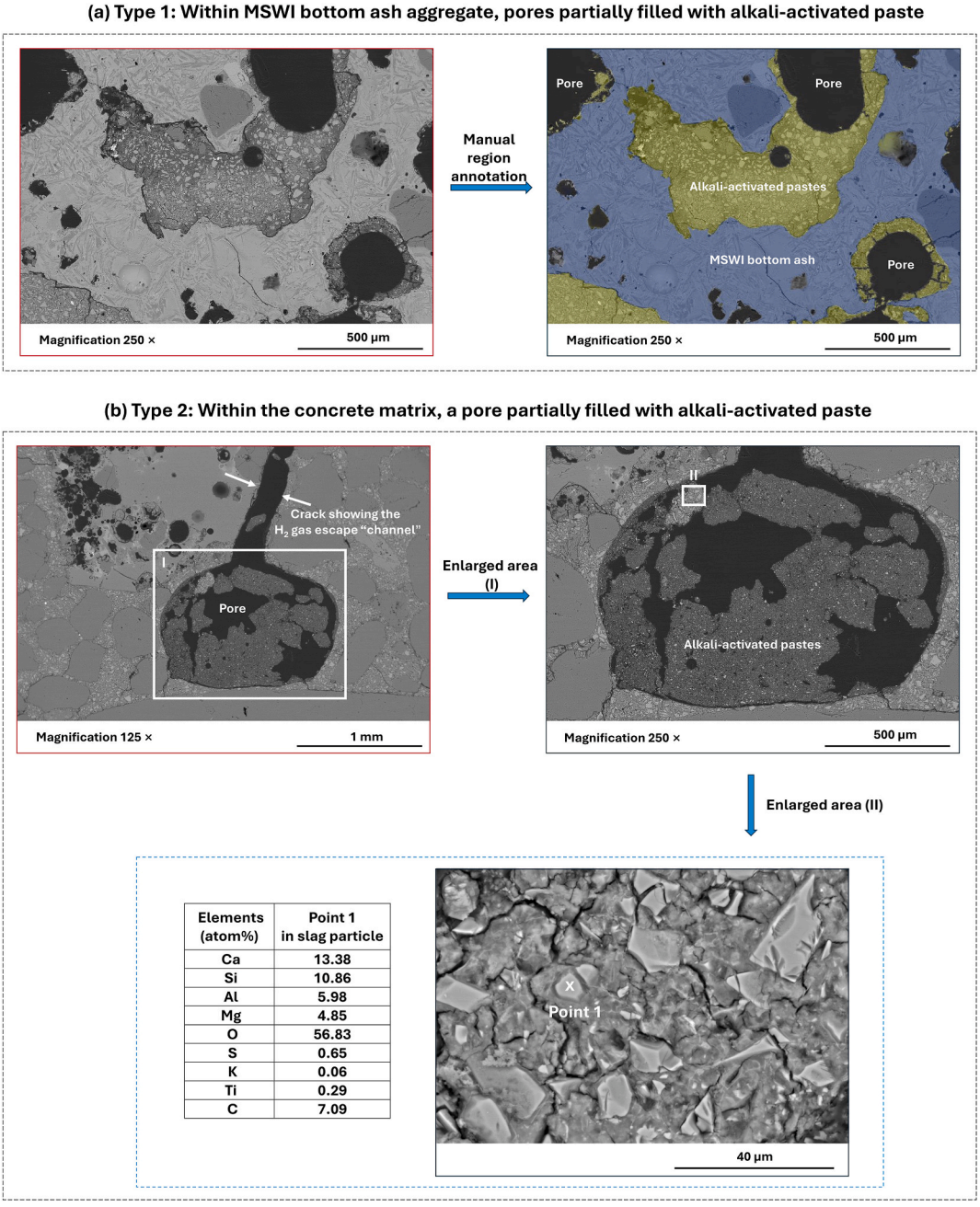

Elements (atom%)	Point 1 in slag particle
Ca	13.38
Si	10.86
Al	5.98
Mg	4.85
O	56.83
S	0.65
K	0.06
Ti	0.29
C	7.09

Fig. 10. SEM-BSE image showing the two types of pores partially filled with alkali-activated pastes in 30BA-AAC.

influence on the final value. It ranges between 0 and 1, where 1 represents a perfect sphere, and lower values indicate irregular or elongated shapes. The pores in the range of 100–300 μm are preferable for enhancing freeze-thaw resistance in foamed concrete [66]. Fig. 9 (b) shows that pores smaller than 300 μm in 30BA-AAC exhibit slightly lower sphericity compared to the reference samples. This reduced sphericity may negatively impact its freeze-thaw resistance. The irregular pores cause higher stress concentrations and weaken structural integrity. In contrast, spherical pores help distribute stress more evenly, potentially enhancing freeze-thaw resistance [67].

Unlike the reference samples, the 30BA-AAC sample contains pores that are partially filled with alkali-activated paste. The formation of this pore morphology is associated with the characteristics of MSWI BA aggregates. Fig. 10 shows two typical examples. Fig. 10 (a) shows a local area of a large MSWI bottom ash aggregate particle. It can be seen that the bottom ash particle is porous, and some of its pores are partially filled with the alkali-activated paste. These partially filled pores may have originally been located on the surface of the bottom ash. When the aggregates came into contact with the paste, the paste penetrated and filled the surface irregularities, resulting in a smoother aggregate surface. Fig. 10 (b) presents a view of the concrete in which the aggregates, pores, and binder matrix are clearly visible. A spherical pore with a narrow neck is located in the binder matrix and is partially filled with alkali-activated paste. Unreacted slag particles are also observed within the paste and were identified based on their elemental composition measured at point 1. Pores with this shape are detrimental to freeze-thaw resistance, as they have channels connecting to other regions of the matrix, indicating that they are open rather than closed. Based on their characteristics, these pores may have formed as a result of the oxidation of metallic Al. MSWI bottom ash aggregates contain metallic Al, which reacts in an alkaline environment, dissolving and releasing hydrogen gas. The gas buildup creates internal pressure, preventing the surrounding paste from forming a solid, continuous structure, which can lead to cracks in the matrix. Once the hydrogen gas is released, it dissipates, leaving behind voids that form observable channels within the matrix (Fig. 10 (b)).

3.2.1.2. Properties of interfacial transition zone. MSWI BA aggregates are heterogeneous, with porosity varying even within a single particle. This variation results in a heterogeneous ITZ surrounding the bottom ash aggregate (Fig. 11). In 30BA-AAC, the ITZ morphology is strongly influenced by the porosity of the attached MSWI bottom ash regions—higher porosity generally results in a weaker ITZ. Unreacted slag particles are also observed in the ITZ, appearing as light grey in color (see labeled particle in Fig. 12 (a)). There are three characteristic interfacial transition zones observed around the bottom ash aggregates.

Type 1: Fig. 12 (a) shows that the ITZ surrounding highly porous regions of MSWI BA aggregates has weak adhesion and contains visible air voids. These voids are likely due to trapped air within the aggregates. When the activator fills the porous structure, it can displace this air, causing it to migrate into the surrounding matrix and leave voids in the ITZ. This process contributes to the weak bond between the aggregate and the matrix.

Type 2: In Fig. 12 (b), this region of the MSWI bottom ash aggregate has lower porosity than the one in Fig. 12 (a). A clear interfacial gap is visible between the MSWI bottom ash aggregate and the surrounding matrix. A crack runs through the entire ITZ. This porous and cracked ITZ forms primarily due to the high water absorption capacity of MSWI BA aggregates. During curing, the absorbed water is gradually released, locally increasing the water-to-binder ratio in the surrounding matrix. This results in higher porosity, weaker interfacial bonding, and greater susceptibility to drying shrinkage and microcracking. A distinct transition is observed in the ITZ. Additionally, as the distance from the MSWI bottom ash aggregate increases, fewer cracks are observed. The matrix becomes denser near the natural aggregates and a more continuous and dense aggregate-matrix interface is observed.

Type 3: Fig. 12 (c) illustrates a well-bonded interface between the dense regions of MSWI BA aggregates and the binder matrix. The bottom ash in this figure has a dense microstructure. Therefore, it behaves more like natural aggregates, contributing to a well-developed interfacial bond. It is worth mentioning that when ground into a fine powder, MSWI bottom ash exhibits reactivity similar to Class F coal fly ash [5,16,38]. The strong adhesion may be due to a partial reaction of the surface layer of the MSWI BA

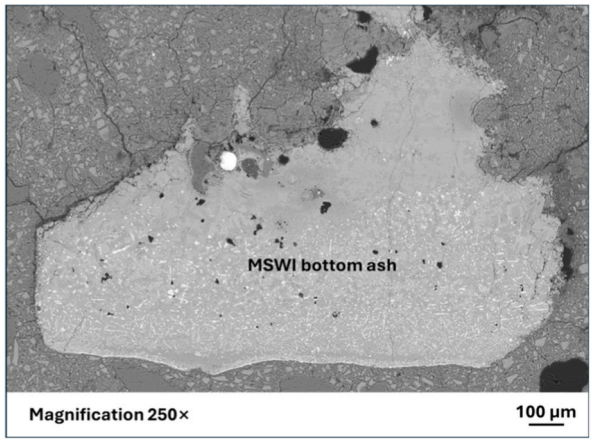

Fig. 11. A representative MSWI bottom ash aggregate in 30BA-AAC, showing variations in porosity across different regions of the particle and the corresponding heterogeneous ITZ.

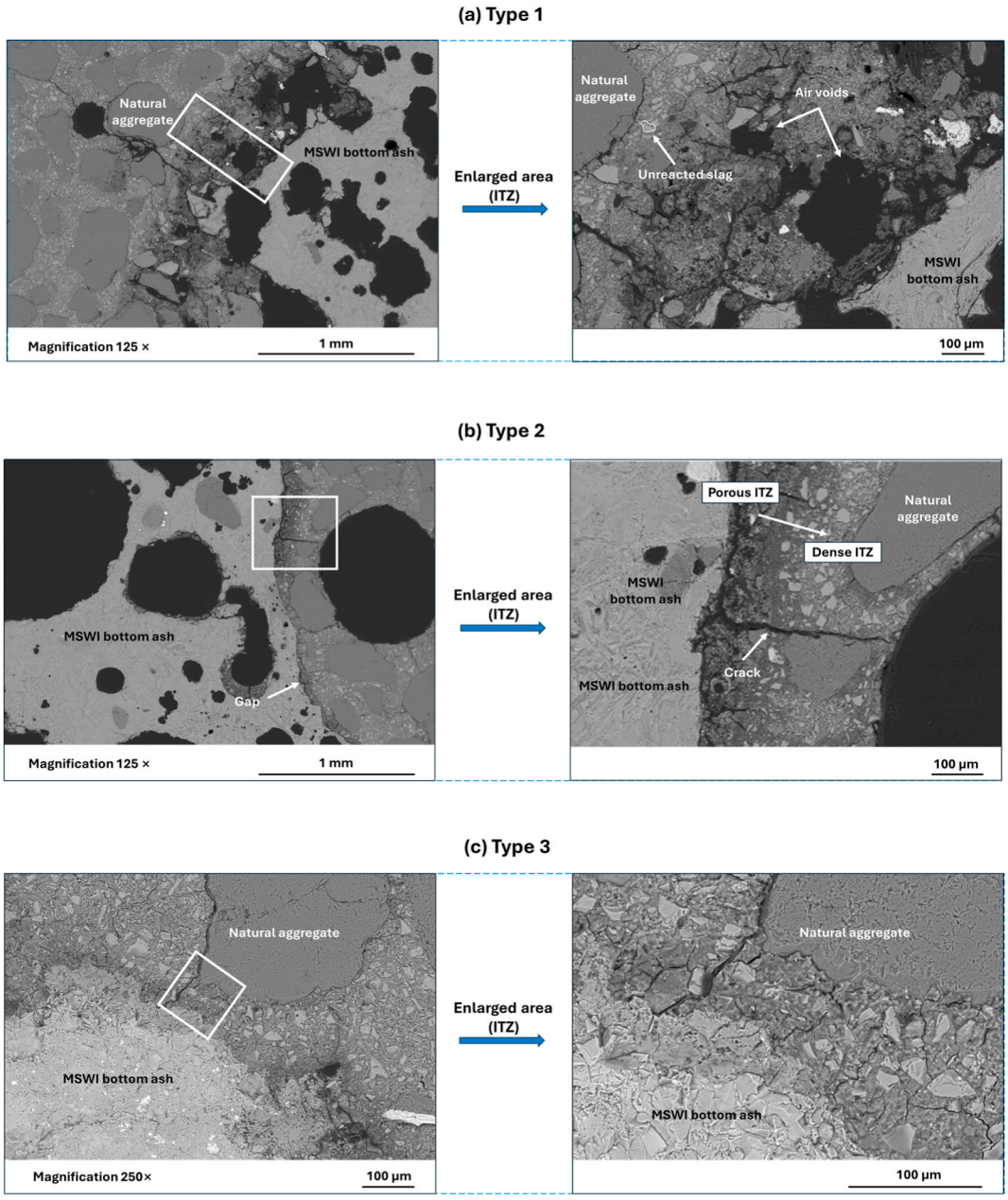

Fig. 12. SEM-BSE images of three distinct interfacial transition zones (ITZs) surrounding regions of MSWI bottom ash aggregates with different porosity in 30BA-AAC.

aggregates, which improves their integration with the alkali-activated matrix.

3.2.2. Mechanical properties

All mechanical properties, including compressive strength, splitting tensile strength, and flexural strength, are presented in Fig. 13. The 28-day results for compressive strength, splitting tensile strength, and flexural strength exhibited consistent trends across all samples. Among these, the 30BA-AAC sample showed the lowest strength, followed by 100NA-AAC, while 100NA-BCC demonstrated the highest strength. It is worth noting that the reference AAC mix in this study was designed with a higher-than-required strength class to compensate for potential strength reductions when replacing natural aggregates with MSWI BA. While this method provides a practical solution under current conditions, it may reduce efficiency in material use and mix design optimization.

Compared to natural aggregates, MSWI bottom ash aggregates have higher surface roughness, which can enhance mechanical interlocking between the binder and aggregates, improving the bond strength in some regions of AAC. However, their high porosity

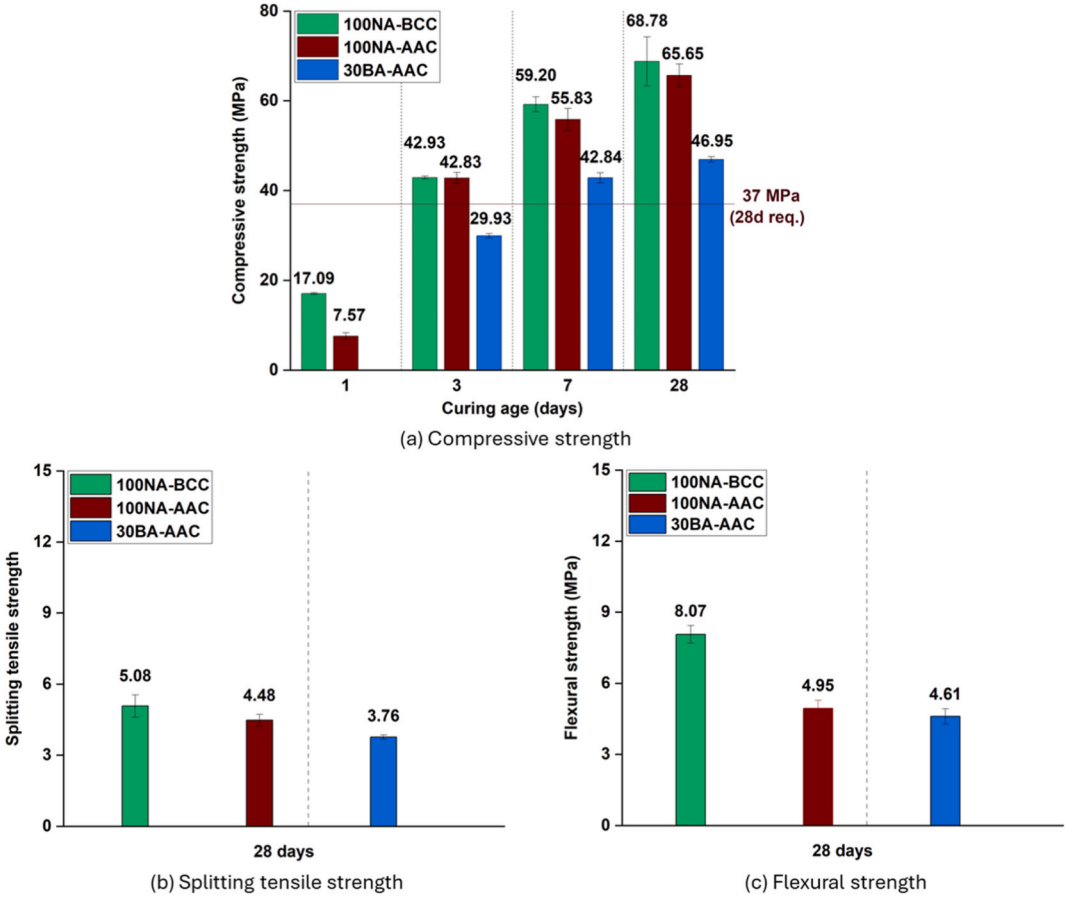

Fig. 13. Compressive, splitting tensile, and flexural strength of reference concrete and concrete containing MSWI bottom ash aggregates.

may also lead to localized weak zones due to increased water absorption and heterogeneous ITZ formation. In the case of 30BA-AAC, the lower mechanical properties can primarily be attributed to its significantly higher total porosity and the increased porosity and cracking in the ITZ compared to reference samples (see Fig. 8 (a)). Although a reduction in strength was observed when natural aggregates were replaced with MSWI BA aggregates, the 28-day strength of alkali-activated concrete still met the C30/37 strength requirements.

A noticeable difference is observed in the 1-day compressive strength. Unlike reference samples, the 30BA-AAC sample did not harden after 1 day. This could be attributed to the partial consumption of NaOH solution from the activator during the pre-treatment of the MSWI BA aggregates. Additionally, the fine particles in MSWI bottom ash, which exhibit reactivity similar to that of Class F fly ash [38], may also consume the alkaline solution. The availability of alkalis, particularly from NaOH solution, is critical for early-age strength development [68]. A reduction in available alkalis hinders the dissolution of precursor, leading to delayed setting and strength gain. The lower early-age strength could potentially be improved through thermal treatment or by increasing the alkalinity of the activator. However, both strategies would increase the environmental impact of the final product. As a result, these approaches were not implemented in this study.

The reduced 28-day compressive, splitting tensile, and flexural strengths of alkali-activated concrete incorporating MSWI BA aggregates can be attributed to their high Los Angeles coefficient, high water absorption, and inclusion of metallic Al. Aggregates with high Los Angeles values exhibit lower abrasion resistance and mechanical durability. Kılıc et al. [69] established a strong negative relationship between the Los Angeles abrasion values of aggregates and the mechanical performance of concrete, including compressive and flexural strengths. The high water absorption of MSWI BA aggregates increases the liquid-to-binder ratio near the aggregate surface, resulting in higher porosity in the interfacial transition zone [70,71]. Additionally, the residual metallic Al in MSWI BA aggregates is initially covered by a protective mineral layer [33]. During the curing process, the activator may dissolve this layer, exposing the Al to react and release hydrogen gas. This gas release further increases porosity and induces stress concentrations in the concrete matrix. These combined effects weaken the ITZ, impairing the bond between the aggregate and the binder. The weakened ITZ and increased porosity hinder the effective transfer of stresses, leading to reductions in compressive, splitting tensile, and flexural strengths. The pore distribution in concrete is discussed in more detail in section 3.2.1.

3.2.3. Freeze-thaw resistance

Fig. 14 shows the surface scaling of concrete samples after 4, 6, 14, and 28 cycles. Concrete typically has low freeze-thaw durability because capillary pores retain water, which freezes and expands at temperatures below 0 °C. This expansion generates hydraulic pressure that exceeds the tensile strength of the concrete, leading to cracking and deterioration. Among the tested samples, the blended cement concrete (100NA-BCC) demonstrated the highest freeze-thaw durability, with total surface scaling of 2.43 kg/m^2 after 28 cycles. Replacing the blended cement matrix with an alkali-activated matrix, as in the natural aggregate alkali-activated concrete (100NA-AAC), reduced the freeze-thaw durability, resulting in surface scaling of 4.52 kg/m^2. The poorer freeze-thaw resistance of 100NA-AAC suggests that existing mix design provisions may require adaptation for alkali-activated concrete. The decline in freeze-thaw durability can be attributed to the dense microstructure of the binder in 100NA-AAC, which mainly contains nanopores smaller than 100 nm [65]. These small pores reduce permeability and hinder the redistribution of water, leading to localized pore saturation. During freezing, the confined water within the capillary pores expands, generating substantial internal stresses and resulting in cracking and progressive damage during freeze-thaw cycles [72].

The substitution of natural aggregates with MSWI BA aggregates in the alkali-activated concrete resulted in reduced freeze-thaw resistance, as evidenced by an increase in surface scaling from 4.52 kg/m^2 to 5.23 kg/m^2 in the conducted tests. The low freeze-thaw resistance of alkali-activated concrete containing MSWI BA aggregates (30BA-AAC) is influenced by several factors. First, the high water absorption capacity of the bottom ash aggregates makes them highly susceptible to damage during freeze-thaw cycles. As the absorbed water freezes and expands, it causes internal cracking and aggregate degradation. Second, the incorporation of MSWI BA aggregates increases the total pore volume in concrete, particularly the number of large pores, significantly enhancing water retention and permeability compared to the reference samples. Although small pores (100–300 μm) are beneficial for freeze-thaw resistance [66], the pores in 30BA-AAC have lower sphericity than those in the reference samples (see Fig. 9 (b)). As a result, their effectiveness in improving freeze-thaw resistance is reduced. Third, the cracks and pores in the ITZ surrounding MSWI BA aggregates (see Fig. 12) weaken the microstructure, further compromising freeze-thaw durability.

3.3. Environmental impacts of AAC incorporating MSWI BA aggregates

Life cycle assessment is conducted to determine whether AAC containing MSWI BA aggregates is a viable environmental alternative to OPC concrete. Fig. 15 illustrates the environmental impacts of various concrete mixtures with similar 28-day compressive strength. More details of these concrete mixtures can be found in Table 2. Among them, 30BA-AAC has the lowest environmental impact in most categories. It performs exceptionally well in terms of GWP, indicating a significantly lower carbon footprint. Among the AAC mixtures, 30BA-AAC has a significantly lower environmental impact than AAC I, II, and III. This reduction is due to its lower activator content, which is achieved by producing zero-slump concrete.

Compared to OPC and CEM III/B concrete, AAC mixtures generally exhibit a lower GWP due to the absence of cement, but they introduce trade-offs in other impact categories due to the use of alkali activators. In OPC and CEM III/B concrete, clinker production is the dominant contributor to environmental impact, particularly in GWP. It is important to note that among all concrete ingredients, aggregates have a minimal contribution to the overall environmental footprint (Fig. 15).

The total Environmental Cost Indicator (ECI) value provides a holistic assessment of a concrete mixture's overall environmental impact. In the ECI calculation, a monetary cost is assigned to each impact category to account for and mitigate its associated

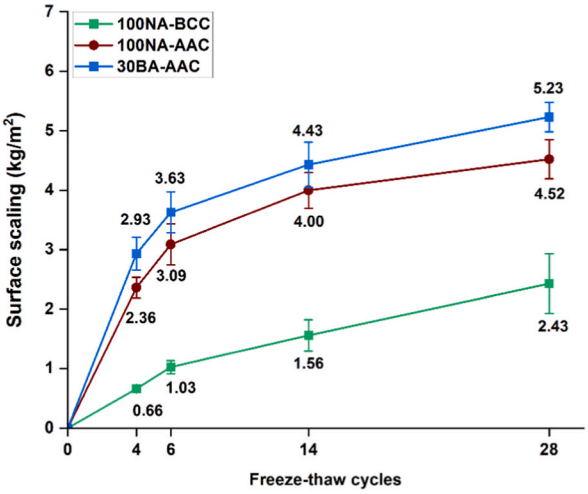

Fig. 14. Surface scaling of reference concrete and concrete containing MSWI bottom ash aggregates during freeze-thaw cycles.

environmental burdens. Among the mixtures studied, 30BA-AAC has the lowest ECI value at €4.56 (see Fig. 16), demonstrating its superior environmental performance. In contrast, OPC I, which has the highest cement content, shows the highest ECI value at €29.55. As shown in Fig. 16, global warming potential (GWP) has the greatest influence on ECI values in cement-based mixtures. In alkali-activated mixtures, GWP and human toxicity potential (HTP) are the two dominant contributors to ECI. The high HTP in alkali-activated mixtures is primarily attributed to the use of activators, particularly water glass.

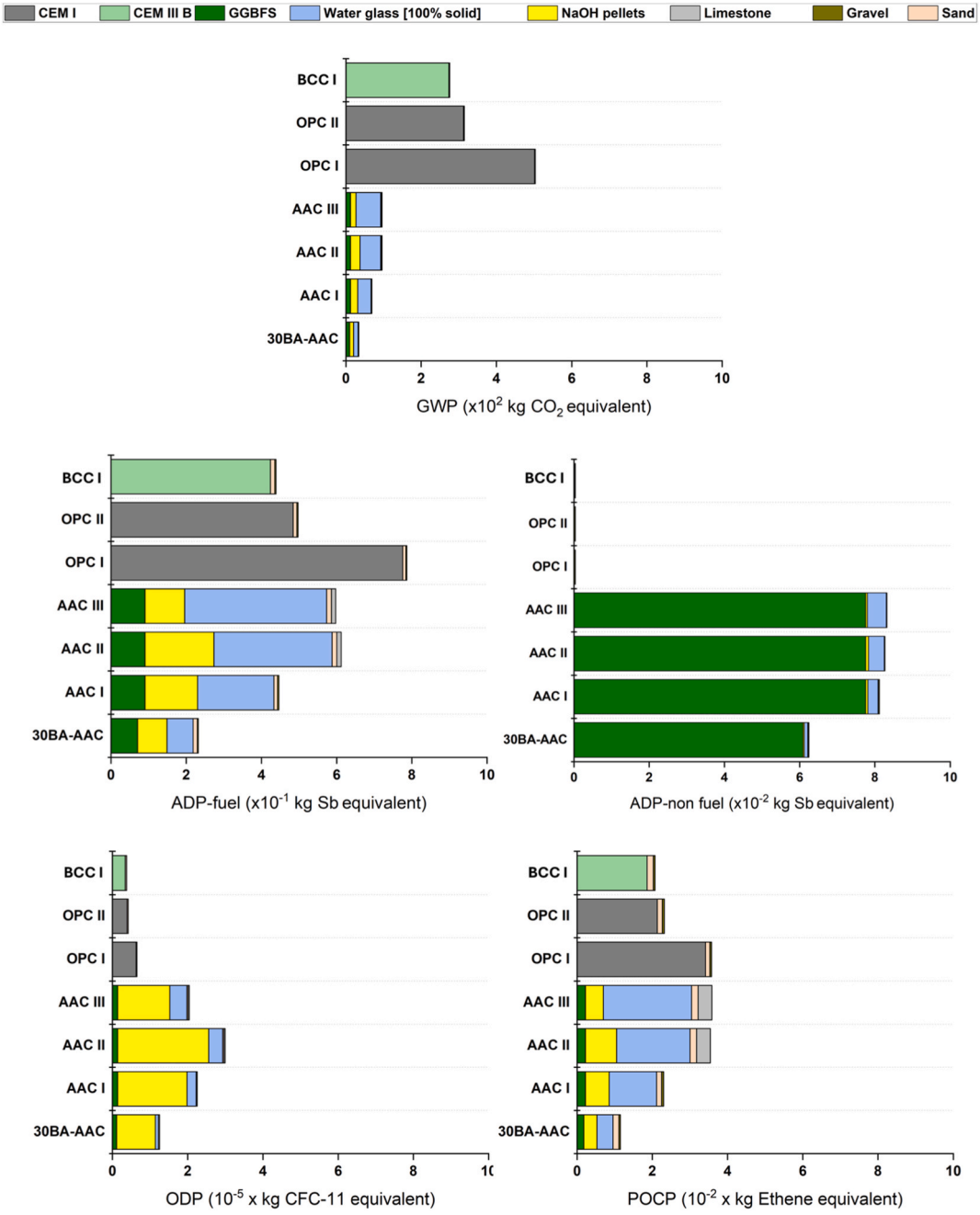

Fig. 15. Environmental impacts of various concrete mixtures (strength class C30/37) across different categories in life cycle assessment (LCA). The abbreviations in this figure represent the following impact categories: GWP stands for global warming potential, ADP for abiotic depletion, ODP for ozone depletion, and POCP for photochemical ozone creation potential, AP stands for acidification potential, EP for eutrophication potential, HTP for human toxicity potential, FAETP for freshwater aquatic ecotoxicity potential, MAETP for marine aquatic ecotoxicity potential, and TAETP for terrestrial ecotoxicity potential.

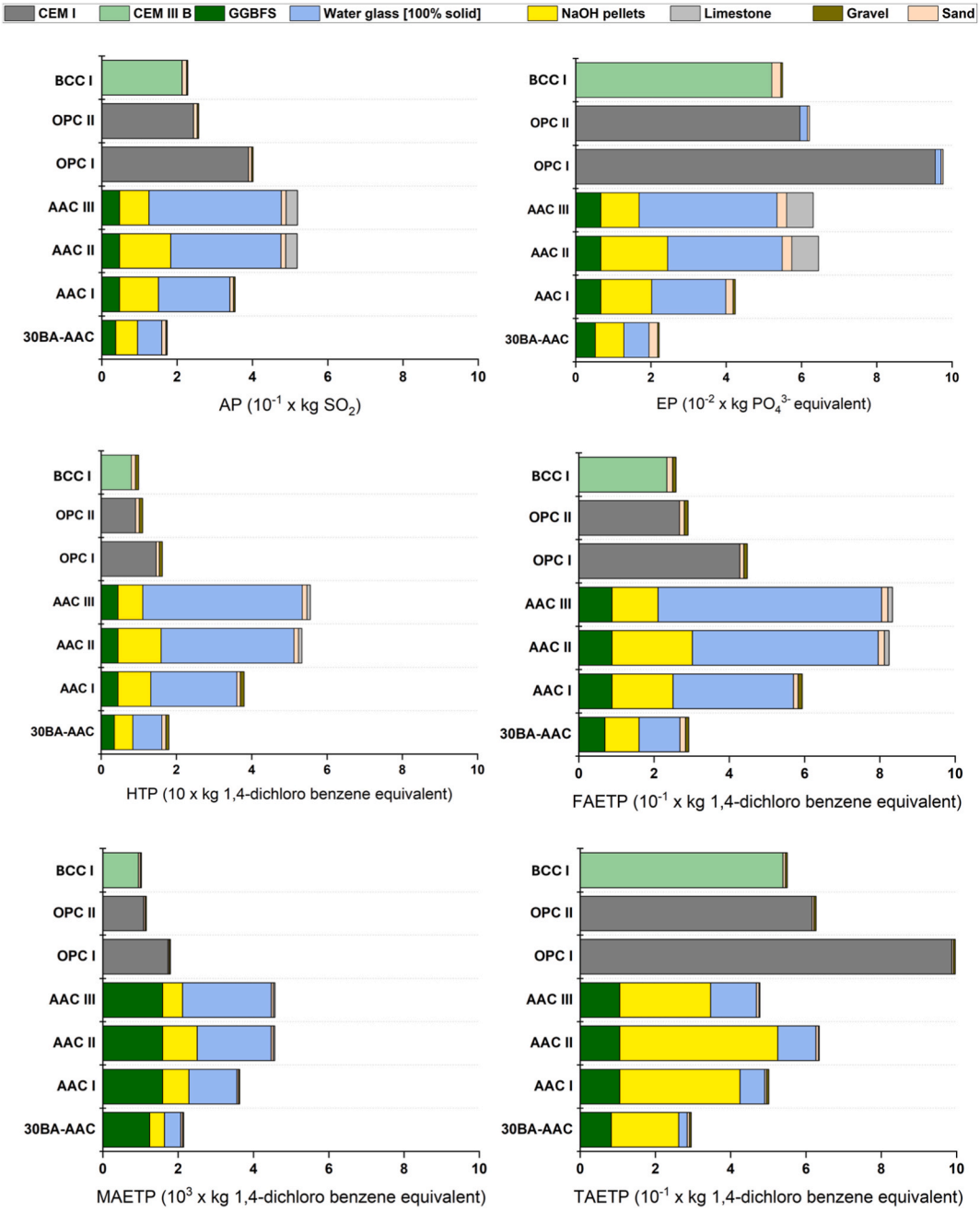

Fig. 15. (*continued*).

3.4. Leaching risks of AAC incorporating MSWI BA aggregates

In the leaching test, concrete samples were crushed into granulates to simulate their end-of-life state. The leaching values were compared with the upper limit for unshaped materials as specified in the Dutch standard. The results (see Table 4) show that the leaching behavior of 30BA-AAC complies with the Soil Quality Decree [73]. This finding indicates that MSWI BA aggregates can be safely incorporated into alkali-activated concrete. The low leaching risk of the developed AAC is attributed to the immobilization effect of the alkali-activated slag matrix, which stabilizes heavy metals within the gel phase, significantly limiting their release and reducing environmental risks [74].

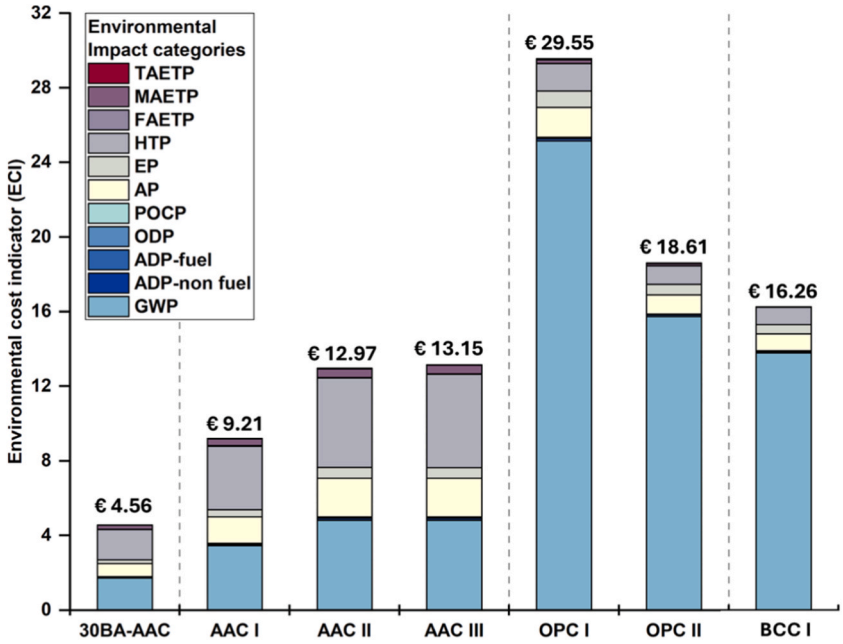

Fig. 16. Contribution of each environmental impact category to the total Environmental Cost Indicator (ECI) per cubic meter of concrete (strength class C30/37) across different mix designs.

Table 4
Leaching test results of 30BA-AAC with regulatory threshold values for comparison.

Elements	30BA-AAC (mg/kg dry solid)	Upper limit value (mg/kg dry solid) [73]
Antimony	0.11	0.32
Arsenic	0.5	0.9
Barium	<0.1	22
Cadmium	<0.007	0.04
Chrome	<0.05	0.63
Cobalt	<0.05	0.54
Copper	<0.05	0.9
Lead	<0.01	2.3
Mercury	0.0023	0.02
Molybdenum	0.22	1
Nickel	<0.01	0.44
Selenium	0.11	0.15
Tin	0.03	0.4
Vanadium	0.47	1.8
Zinc	<0.2	4.5
Fluoride	5.5	18
Bromide	<0.8	20
Chloride	69	616
Sulfate	450	2430

4. Conclusions and recommendations

This study presents the development of a new alkali-activated concrete (AAC) incorporating municipal solid waste incineration (MSWI) bottom ash (BA) as coarse aggregate, along with a comprehensive assessment of its pore structure, engineering performance, and environmental performance. The key findings and recommendations are presented below.

- Although the MSWI BA aggregates used in this study were obtained from a single incineration facility, they exhibit characteristics commonly associated with such materials, including high porosity, mechanical weakness, and residual metallic aluminum (Al). The aggregates also display significant heterogeneity, with individual particles showing a wide range of porosity levels. When incorporated into AAC, highly porous MSWI BA particles tend to generate a more porous and microcracked interfacial transition zone (ITZ), influencing both the local microstructure and the overall pore network of the concrete. The NaOH-based pre-treatment

effectively mitigates Al-induced expansion and surface cracking; however, residual metallic Al still contributes to entrapped porosity within AAC.

- AAC with 30 wt% of the coarse aggregates replaced by NaOH-treated MSWI BA maintains strength class C30/37, demonstrating that treated MSWI BA aggregates can be incorporated while preserving sufficient mechanical performance for structural-grade AAC. While BA replacement alone offers limited sustainability gains, the integration of treated MSWI BA within AAC produces a mixture that is more sustainable than Ordinary Portland Cement (OPC) concrete, CEM III/B concrete, and other AAC mixtures of similar strength levels reported in the literature. Leaching results further confirm the environmental safety of the developed mixture, showing no significant release of harmful contaminants.
- In the absence of AAC-specific design guidelines, conventional OPC-based provisions were used. Even so, the reference AAC containing only natural aggregates exhibited insufficient freeze-thaw resistance, and the partial replacement with MSWI BA further increased surface scaling. These results highlight the need for design criteria tailored to AAC.
- Freeze-thaw performance of AAC is strongly influenced by the inherent pore structure of MSWI BA and the presence of residual metallic Al. The porous structure tends to introduce excessive and irregularly shaped pores, increasing water retention and susceptibility to internal cracking during freezing cycles. Although metallic Al can generate air voids, the resulting pore system is not inherently beneficial for freeze-thaw resistance unless the size, shape, and distribution of the voids are adequately controlled. Given these limitations under freeze-thaw conditions, AAC incorporating MSWI BA as coarse aggregate is best suited for indoor applications or outdoor environments with minimal freezing exposure.
- Future investigations should quantify the porous fraction of MSWI BA aggregates (e.g., via water absorption, density-based segregation, or X-ray CT), as this would improve assessment of potential damage mechanisms and enhance quality control. Establishing pre-treatment threshold criteria for MSWI BA aggregates (e.g., maximum allowable water absorption or acceptable post-treatment H_2 gas release under alkaline conditions) would further support more consistent performance.
- Future work may assess the feasibility of using finely ground MSWI bottom ash as a reactive coating for coarse bottom ash aggregates, with the objective of promoting pore refinement in accessible (near-surface) porosity through in-situ gel formation prior to their incorporation into alkali-activated matrix. This pore-filling effect could reduce the water demand of the aggregates and improve the quality of the aggregate-matrix interface.
- Future studies could also focus on an integrated mechanical-durability-environmental optimization, where LCA results are correlated with strength and durability performance to more accurately assess the overall sustainability of AAC mixtures.

CRediT authorship contribution statement

Boyu Chen: Writing – review & editing, Writing – original draft, Visualization, Methodology, Formal analysis, Conceptualization, Data curation. **Ivana Mariam Paul:** Methodology, Investigation, Data curation, Formal analysis, Visualization. **Luiz Miranda de Lima:** Writing – review & editing, Methodology. **Patrick Holthuizen:** Writing – review & editing, Investigation, Formal analysis. **Shan He:** Writing – review & editing, Investigation. **Burcu Aytekin:** Writing – review & editing, Investigation, Writing – original draft. **Yu Zeng:** Writing – review & editing, Visualization, Formal analysis, Writing – original draft. **Guang Ye:** Writing – review & editing, Supervision.

Declaration of competing interest

The authors declare that they have no known competing financial interests or personal relationships that could have appeared to influence the work reported in this paper.

Acknowledgments

This work was supported by the funding received from the European Union's Horizon Europe research and innovation programme under grant agreement No 101058162 (AshCycle). Mineralz (Part of Renewi) is acknowledged for providing MSWI bottom ash used in this research. Arjan Thijssen, Ton Blom, Maiko van Leeuwen, and John van de Berg, from the Stevin lab and Microlab at the Faculty of Civil Engineering and Geosciences, Delft University of Technology, are acknowledged for their support for all the experiments.

Appendix

Table A 1
Life cycle inventory data of raw materials used in the preparation of concrete binder.

Environmental impact category	Unit	GGBFS [Eco$_2$ cem]	CEM I 42.5 N [ENCI/Heidelberg Cement]	CEM III/B 42.5 N [ENCI/Heidelberg Cement]
GWP	kg CO_2 equivalent	3.03E-02	3.71E-08	7.82E-01
ADP-non fuel	kg Sb equivalent	1.94E-04	7.62E-04	6.80E-08

(*continued on next page*)

Table A 1 (*continued*)

Environmental impact category	Unit	GGBFS [Eco$_2$ cem]	CEM I 42.5 N [ENCI/Heidelberg Cement]	CEM III/B 42.5 N [ENCI/Heidelberg Cement]
ADP-fuel	kg Sb equivalent	2.26E-04	2.70E-01	1.21E-03
ODP	kg CFC-11 equivalent	3.47E-09	8.10E-09	9.89E-09
POCP	kg Ethene equivalent	5.68E-06	3.56E-05	5.33E-05
AP	kg SO_2 equivalent	1.17E-04	4.02E-04	6.08E-04
EP	kg PO_4^{3-} equivalent	1.67E-05	6.93E-05	1.49E-04
HTP	kg 1,4-dichloro benzene equivalent	1.12E-02	1.40E-02	2.29E-02
FAETP	kg 1,4-dichloro benzene equivalent	2.20E-04	3.03E-04	6.68E-04
MAETP	kg 1,4-dichloro benzene equivalent	3.97E+00	1.15E+00	2.70E+00
TAETP	kg 1,4-dichloro benzene equivalent	2.62E-04	3.58E-04	1.54E-03

Table A 2
Life cycle inventory data of the raw materials used to prepare activators [60].

Environmental impact category	Unit	NaOH pellets	Water glass (100 wt% pure)
GWP	kg CO_2 equivalent	8.73E-01	9.53E-01
ADP-non fuel	kg Sb equivalent	2.66E-05	7.20E-05
ADP-fuel	kg Sb equivalent	6.23E-03	5.48E-03
ODP	kg CFC-11 equivalent	8.23E-07	6.50E-08
POCP	kg Ethene equivalent	2.81E-04	3.40E-04
AP	kg SO_2 equivalent	4.64E-03	5.10E-03
EP	kg PO_4^{3-} equivalent	6.04E-04	5.32E-04
HTP	kg 1,4-dichloro benzene equivalent	3.91E-01	6.15E-01
FAETP	kg 1,4-dichloro benzene equivalent	7.26E-03	8.63E-03
MAETP	kg 1,4-dichloro benzene equivalent	3.11E+01	3.43E+01
TAETP	kg 1,4-dichloro benzene equivalent	1.43E-02	1.77E-03

Table A 3
Life cycle inventory data of aggregates used in concrete mix design [60].

Environmental impact category	Unit	Aggregates			
		MSWI bottom ash	Gravel (4–8 mm & 8–16 mm)	Limestone (crushed)	Sand (0–4 mm)
GWP	kg CO_2 equivalent	0	4.79E-04	2.23E-03	2.26E-03
ADP-non fuel	kg Sb equivalent	0	1.99E-07	2.02E-08	2.03E-07
ADP-fuel	kg Sb equivalent	0	2.94E-06	1.38E-05	1.48E-05
ODP	kg CFC-11 equivalent	0	3.09E-11	3.38E-10	3.79E-10
POCP	kg Ethene equivalent	0	4.72E-07	4.27E-06	2.03E-06
AP	kg SO_2 equivalent	0	3.32E-06	3.51E-05	1.51E-05
EP	kg PO_4^{3-} equivalent	0	4.69E-07	8.23E-06	2.99E-06
HTP	kg 1,4-dichloro benzene equivalent	0	8.47E-04	1.05E-03	1.42E-03
FAETP	kg 1,4-dichloro benzene equivalent	0	9.09E-06	1.43E-05	1.92E-05
MAETP	kg 1,4-dichloro benzene equivalent	0	2.76E-02	4.83E-02	6.34E-02
TAETP	kg 1,4-dichloro benzene equivalent	0	4.82E-06	2.82E-06	7.94E-06

Table A 4
Environmental impact categories and their respective shadow cost [60].

Environmental impact category	Abbreviation	Unit	Shadow cost(€) per kg equivalents
Global warming potential	GWP	kg CO_2 equivalent	€0.05
Abiotic depletion potential (non-fuel)	ADP-non fuel	kg Sb equivalent	€0.16
Abiotic depletion potential -fuel	ADP-fuel	kg Sb equivalent	€0.16
Ozone layer depletion potential	ODP	kg CFC-11 equivalent	€30.00
photochemical ozone creation potential	POCP	kg Ethene equivalent	€2.00
Acidification potential	AP	kg SO_2 equivalent	€4.00
Eutrophication potential	EP	kg PO_4^{3-} equivalent	€9.00
Human toxicity potential	HTP	kg 1,4-dichloro benzene equivalent	€0.09
Freshwater aquatic ecotoxicity potential	FAETP	kg 1,4-dichloro benzene equivalent	€0.03
Marine aquatic ecotoxicity potential	MAETP	kg 1,4-dichloro benzene equivalent	€0.00
Terrestrial ecotoxicity potential	TAETP	kg 1,4-dichloro benzene equivalent	€0.06

Data availability

Data will be made available on request.

References

[1] C.R. Gagg, Cement and concrete as an engineering material: an historic appraisal and case study analysis, Eng. Fail. Anal. 40 (2014) 114–140, https://doi.org/10.1016/j.engfailanal.2014.02.004.
[2] P. Hewlett, M. Liska, Lea's Chemistry of Cement and Concrete, Butterworth-Heinemann, 2019.
[3] R.M. Andrew, Global CO 2 emissions from cement production, Earth Syst. Sci. Data 10 (2018) 195–217.
[4] B. Estanqueiro, J. Dinis Silvestre, J. de Brito, M. Duarte Pinheiro, Environmental life cycle assessment of coarse natural and recycled aggregates for concrete, Eur. J. Environ. Civ. Eng. 22 (2018) 429–449, https://doi.org/10.1080/19648189.2016.1197161.
[5] B. Chen, P. Perumal, F. Aghabeyk, A. Adediran, M. Illikainen, G. Ye, Advances in using municipal solid waste incineration (MSWI) bottom ash as precursor for alkali-activation materials: a critical review, Resour. Conserv. Recycl. 204 (2024) 107516, https://doi.org/10.1016/j.resconrec.2024.107516.
[6] J.L. Provis, A. Palomo, C. Shi, Advances in understanding alkali-activated materials, Cement Concr. Res. 78 (2015) 110–125, https://doi.org/10.1016/j.cemconres.2015.04.013.
[7] A. Wang, Y. Zheng, Z. Zhang, K. Liu, Y. Li, L. Shi, D. Sun, The durability of alkali-activated materials in comparison with ordinary Portland cements and concretes: a review, Engineering 6 (2020) 695–706, https://doi.org/10.1016/j.eng.2019.08.019.
[8] Y. Ding, J.-G. Dai, C.-J. Shi, Mechanical properties of alkali-activated concrete: a state-of-the-art review, Constr. Build. Mater. 127 (2016) 68–79, https://doi.org/10.1016/j.conbuildmat.2016.09.121.
[9] J.M. Chimenos, M. Segarra, M.A. Fernandez, F. Espiell, Characterization of the bottom ash in municipal solid waste incinerator, J. Hazard. Mater. Adv. 64 (1999) 211–222.
[10] M. Šyc, F.G. Simon, J. Hykš, R. Braga, L. Biganzoli, G. Costa, V. Funari, M. Grosso, Metal recovery from incineration bottom ash: State-of-the-art and recent developments, J. Hazard. Mater. 393 (2020) 122433, https://doi.org/10.1016/j.jhazmat.2020.122433.
[11] Y. Xia, P. He, L. Shao, H. Zhang, Metal distribution characteristic of MSWI bottom ash in view of metal recovery, J. Environ. Sci. (China). 52 (2017) 178–189, https://doi.org/10.1016/j.jes.2016.04.016.
[12] Eurostat (Statistical Office of the European Communities), Municipal waste statistics. https://ec.europa.eu/eurostat/statistics-explained/index.php?title=Municipal_waste_statistics#Municipal_waste_generation, 2023.
[13] United States Environmental Protection Agency (US EPA), National overview: facts and figures on materials, wastes and recycling. https://www.epa.gov/facts-and-figures-about-materials-waste-and-recycling/national-overview-facts-and-figures-materials, 2022.
[14] National Bureau of Statistics of China (NBS), Urban garbage collection and disposal situation. https://data.stats.gov.cn/easyquery.htm?cn=E0103, 2022.
[15] International Renewable Energy Agency (IRENA), Renewable capacity Statistics 2022. https://www.irena.org/-/media/Files/IRENA/Agency/Publication/2022/Apr/IRENA_RE_Capacity_Statistics_2022.pdf?rev=460f190dea15442eba8373d9625341ae, 2022.
[16] B. Chen, P. Perumal, M. Illikainen, G. Ye, A review on the utilization of municipal solid waste incineration (MSWI) bottom ash as a mineral resource for construction materials, J. Build. Eng. (2023) 106386, https://doi.org/10.1016/j.jobe.2023.106386.
[17] A. Keulen, A. Van Zomeren, P. Harpe, W. Aarnink, H.A.E. Simons, H.J.H. Brouwers, High performance of treated and washed MSWI bottom ash granulates as natural aggregate replacement within earth-moist concrete, Waste Manag. 49 (2016) 83–95, https://doi.org/10.1016/j.wasman.2016.01.010.
[18] X. Dou, F. Ren, M.Q. Nguyen, A. Ahamed, K. Yin, W.P. Chan, V.W.C. Chang, Review of MSWI bottom ash utilization from perspectives of collective characterization, treatment and existing application, Renew. Sustain. Energy Rev. 79 (2017) 24–38, https://doi.org/10.1016/j.rser.2017.05.044.
[19] B. Verbinnen, P. Billen, J. Van Caneghem, C. Vandecasteele, Recycling of MSWI bottom ash: a review of chemical barriers, engineering applications and treatment technologies, Waste Biomass Valoriz. 8 (2017) 1453–1466, https://doi.org/10.1007/s12649-016-9704-0.
[20] D. Xuan, P. Tang, C.S. Poon, Limitations and quality upgrading techniques for utilization of MSW incineration bottom ash in engineering applications–A review, Constr. Build. Mater. 190 (2018) 1091–1102.
[21] S. Zhou, H. Luo, B. Feng, W. Zheng, C. Zeng, W. Zhang, J. Liu, F. Xing, Research on using municipal solid waste incineration bottom ash for cement-stabilized macadam, Constr. Build. Mater. 425 (2024) 135850, https://doi.org/10.1016/j.conbuildmat.2024.135850.
[22] J. Yao, H. Song, W. Ling, Z. Yang, Effects of municipal solid waste incineration bottom ash on corrosion resistance of cement mortar, Constr. Build. Mater. 453 (2024) 139088, https://doi.org/10.1016/j.conbuildmat.2024.139088.
[23] A.W. Wong, M.A.A. Aldahdooh, K.H. Lem, S.Y. Looi, M.J.K. Bashir, C.A. Ng, Utilization of thermal plasma decomposed municipal solid waste bottom ash as partial cement and fine aggregates replacements on cement mortar properties, Constr. Build. Mater. 464 (2025) 140142, https://doi.org/10.1016/j.conbuildmat.2025.140142.
[24] J. Liu, Y. Wu, L. Cheng, H. Jin, J. Liu, F. Xing, Recycling of municipal solid waste incineration bottom ash (MSWIBA) particles into natural fine sands for sustainable engineering cementitious composites, Constr. Build. Mater. 418 (2024) 135500, https://doi.org/10.1016/j.conbuildmat.2024.135500.
[25] J. Lu, X. Yang, Y. Lai, J. Gao, Y. Wang, F. Deng, Z. Zhang, Mechanical and microscopic properties of concretes made with municipal solid waste incinerator bottom ash (MSWIBA) exposed to freeze-thaw cycles, Constr. Build. Mater. 452 (2024) 138864, https://doi.org/10.1016/j.conbuildmat.2024.138864.
[26] Q. Wang, H. Chu, F. Li, Incorporating incineration bottom ash in environmentally friendly ultra-high performance concrete: impact on mechanical properties, durability, and environmental benefits, Constr. Build. Mater. 481 (2025) 141640, https://doi.org/10.1016/j.conbuildmat.2025.141640.
[27] J. Bawab, J. Khatib, S. Kenai, M. Sonebi, A review on cementitious materials including municipal solid waste incineration bottom ash (MSWI-BA) as aggregates, Buildings 11 (2021) 179.
[28] X. Gao, B. Yuan, Q.L. Yu, H.J.H. Brouwers, Characterization and application of municipal solid waste incineration (MSWI) bottom ash and waste granite powder in alkali activated slag, J. Clean. Prod. 164 (2017) 410–419, https://doi.org/10.1016/j.jclepro.2017.06.218.
[29] S. Casanova, R.V. Silva, J. de Brito, M.F.C. Pereira, Mortars with alkali-activated municipal solid waste incinerator bottom ash and fine recycled aggregates, J. Clean. Prod. 289 (2021), https://doi.org/10.1016/j.jclepro.2020.125707.
[30] C. Wang, X. Zhao, X. Zhang, J. Zhao, Y. Jin, S. Liu, Y. Zhao, Study of waste incineration bottom ash as fine aggregate applied to green alkali-activated bottom ash-slag concrete: mechanical properties, microstructure, durability, Constr. Build. Mater. 449 (2024) 138484, https://doi.org/10.1016/j.conbuildmat.2024.138484.
[31] E. Loginova, D.S. Volkov, P.M.F. van de Wouw, M.V.A. Florea, H.J.H. Brouwers, Detailed characterization of particle size fractions of municipal solid waste incineration bottom ash, J. Clean. Prod. 207 (2019) 866–874, https://doi.org/10.1016/j.jclepro.2018.10.022.
[32] Y. Cheng, G. Gao, L. Chen, W. Du, W. Mu, Y. Yan, H. Sun, Physical and mechanical study of municipal solid waste incineration (MSWI) bottom ash with different particle size distribution, Constr. Build. Mater. 416 (2024) 135137.
[33] B. Chen, J. Chen, F.F. de Mendonça Filho, Y. Sun, M.B. van Zijl, O. Copuroglu, G. Ye, Characterization and mechanical removal of metallic aluminum (Al) embedded in weathered municipal solid waste incineration (MSWI) bottom ash for application as supplementary cementitious material, Waste Manag. 176 (2024) 128–139, https://doi.org/10.1016/j.wasman.2024.01.031.
[34] G.V.D. Wegen, U. Hofstra, J. Speerstra, G. van der Wegen, U. Hofstra, J. Speerstra, G.V.D. Wegen, U. Hofstra, J. Speerstra, Upgraded MSWI bottom ash as aggregate in concrete, Waste Biomass Valoriz. 4 (2013) 737–743, https://doi.org/10.1007/s12649-013-9255-6.
[35] B. Chen, G. Ye, Enhancing the reaction of municipal solid waste incineration (MSWI) bottom ash in blast furnace slag-based alkali-activated blends: a novel strategy and underlying mechanism, Cem. Concr. Compos. 160 (2025) 106056, https://doi.org/10.1016/j.cemconcomp.2025.106056.
[36] C. Shi, Y. Li, J. Zhang, W. Li, L. Chong, Z. Xie, Performance enhancement of recycled concrete aggregate – a review, J. Clean. Prod. 112 (2016) 466–472, https://doi.org/10.1016/j.jclepro.2015.08.057.

[37] C.J. Lynn, R.K. Dhir Obe, G.S. Ghataora, Municipal incinerated bottom ash characteristics and potential for use as aggregate in concrete, Constr. Build. Mater. 127 (2016) 504–517, https://doi.org/10.1016/j.conbuildmat.2016.09.132.
[38] B. Chen, Y. Zuo, S. Zhang, L.M. de Lima Junior, X. Liang, Y. Chen, M.B. van Zijl, G. Ye, Reactivity and leaching potential of municipal solid waste incineration (MSWI) bottom ash as supplementary cementitious material and precursor for alkali-activated materials, Constr. Build. Mater. 409 (2023) 133890, https://doi.org/10.1016/j.conbuildmat.2023.133890.
[39] NEN-EN 933-1, Tests for geometrical properties of aggregates - part 1: determination of particle size distribution - sieving method. https://connect.nen.nl/Standard/Detail/167446?compId=10037&collectionId=0, 2012.
[40] NEN-EN 1097-6, Tests for Mechanical and Physical Properties of Aggregates - Part 6: Determination of Particle Density and Water Absorption, 2022.
[41] NEN-EN 1097-3, Tests for mechanical and physical properties of aggregates - part 3: determination of loose bulk density and voids. https://connect.nen.nl/Standard/Detail/29059?compId=10037&collectionId=0, 1998.
[42] NEN-EN 1097-2, Tests for mechanical and physical properties of aggregates - part 2: methods for the determination of resistance to fragmentation. https://connect.nen.nl/Standard/Detail/3630227?compId=10037&collectionId=0, 2020.
[43] B. Chen, J. Wang, Experimental study on the durability of alkali-activated slag concrete after freeze-thaw cycle, Adv. Mater. Sci. Eng. 2021 (2021) 1–19, https://doi.org/10.1155/2021/9915639.
[44] NEN-EN 206, Concrete - Specification, Performance, Production and Conformity, 2021.
[45] NEN-EN 933-1, Tests for geometrical properties of aggregates - part 1: determination of particle size distribution-Sieving method. https://connect.nen.nl/Standard/Detail/167446?compId=10037&collectionId=0, 2012.
[46] Y. Sun, B. Chen, S. Zhang, K. Blom, M. Luković, G. Ye, Characterization, pre-treatment, and potential applications of fine MSWI bottom ash as a supplementary cementitious material, Constr. Build. Mater. 421 (2024) 135769, https://doi.org/10.1016/j.conbuildmat.2024.135769.
[47] NEN-EN 12620, Aggregates for concrete. https://connect.nen.nl/Standard/Detail/207757?compId=10037&collectionId=0, 2015.
[48] N. Otsu, A threshold selection method from gray-level histograms, IEEE Trans. Syst. Man Cybern. 9 (1979) 62–66, https://doi.org/10.1109/TSMC.1979.4310076.
[49] NEN-EN 12390-3, Testing hardened concrete - part 3: compressive strength of test specimens. https://www.nen.nl/en/nen-en-12390-3-2019-en-260976, 2019.
[50] NEN-EN 12390-6, Testing hardened concrete - part 6: tensile splitting strength of test specimens. https://www.nen.nl/en/nen-en-12390-6-2009-en-142119, 2009.
[51] NEN-EN 14651, Test method for metallic fibered concrete - measuring the flexural tensile strength (limit or proportionality (LOP), residual). https://www.nen.nl/en/nen-en-14651-2005-a1-2007-en-120650, 2007.
[52] NVN-CEN/TS 12390-9, Testing hardened concrete - part 9: freeze-thaw resistance with de-icing salts - scaling. https://www.nen.nl/en/nvn-cen-ts-12390-9-2016-en-228436, 2016.
[53] ISO 14040, Environmental management - life cycle assessment - principles and framework. https://connect.nen.nl/Standard/Detail/107792?compId=10037&collectionId=0, 2006.
[54] NEN-EN 15804, Sustainability of construction works - environmental product declarations - core rules for the product category of construction products. https://connect.nen.nl/Standard/Detail/3621354?compId=10037&collectionId=0, 2019.
[55] M.N.S. Hadi, N.A. Farhan, M.N. Sheikh, Design of geopolymer concrete with GGBFS at ambient curing condition using Taguchi method, Constr. Build. Mater. 140 (2017) 424–431, https://doi.org/10.1016/j.conbuildmat.2017.02.131.
[56] A.A. Aliabdo, A.E.M. Abd Elmoaty, M.A. Emam, Factors affecting the mechanical properties of alkali activated ground granulated blast furnace slag concrete, Constr. Build. Mater. 197 (2019) 339–355, https://doi.org/10.1016/j.conbuildmat.2018.11.086.
[57] A. Souto-Martinez, E.A. Delesky, K.E.O. Foster, W. V Srubar, A mathematical model for predicting the carbon sequestration potential of ordinary portland cement (OPC) concrete, Constr. Build. Mater. 147 (2017) 417–427, https://doi.org/10.1016/j.conbuildmat.2017.04.133.
[58] M. Shariq, J. Prasad, A. Masood, Effect of GGBFS on time dependent compressive strength of concrete, Constr. Build. Mater. 24 (2010) 1469–1478, https://doi.org/10.1016/j.conbuildmat.2010.01.007.
[59] R. Mors, H. Jonkers, Effect on concrete surface water absorption upon addition of lactate derived agent, Coatings 7 (2017) 51.
[60] Nibe EPD. https://www.nibe-sustainability-experts.com/en/epd-tool, 2025.
[61] M. Dorland, Development of a process for improved integration of environmental cost indicator in construction projects. http://essay.utwente.nl/98414/, 2024.
[62] B. Chen, P. Perumal, C. Liu, Y. Chen, C. Chang, M. Pavlin, D. Kvočka, V. Ducman, T. Luukkonen, M. Illikainen, G. Ye, Municipal solid waste incineration (MSWI) bottom ash-blended cementitious materials: performance, challenges, and potential solutions, Crit. Rev. Environ. Sci. Technol. 55 (2025) 1506–1533, https://doi.org/10.1080/10643389.2025.2548287.
[63] NEN 7375, Leaching Characteristics - Determination of the Leaching of Inorganic Components from Moulded or Monolitic Materials with a Diffusion Test - Solid Earthy and Stony Materials, 2004.
[64] NEN-EN 12620, Aggregates for concrete. https://connect.nen.nl/Standard/Detail/121916?compId=10037&collectionId=0, 2008.
[65] S. Chen, S. Ruan, Q. Zeng, Y. Liu, M. Zhang, Y. Tian, D. Yan, Pore structure of geopolymer materials and its correlations to engineering properties: a review, Constr. Build. Mater. 328 (2022) 127064, https://doi.org/10.1016/j.conbuildmat.2022.127064.
[66] C. Sun, Y. Zhu, J. Guo, Y. Zhang, G. Sun, Effects of foaming agent type on the workability, drying shrinkage, frost resistance and pore distribution of foamed concrete, Constr. Build. Mater. 186 (2018) 833–839, https://doi.org/10.1016/j.conbuildmat.2018.08.019.
[67] Y. Su, J. Zhu, X. Long, L. Zhao, C. Chen, C. Liu, Statistical effects of pore features on mechanical properties and fracture behaviors of heterogeneous random porous materials by phase-field modeling, Int. J. Solid Struct. 264 (2023) 112098, https://doi.org/10.1016/j.ijsolstr.2022.112098.
[68] D. Ravikumar, N. Neithalath, Effects of activator characteristics on the reaction product formation in slag binders activated using alkali silicate powder and NaOH, Cem. Concr. Compos. 34 (2012) 809–818, https://doi.org/10.1016/j.cemconcomp.2012.03.006.
[69] A. Kılıç, C.D. Atiş, A. Teymen, O. Karahan, F. Özcan, C. Bilim, M. Özdemir, The influence of aggregate type on the strength and abrasion resistance of high strength concrete, Cem. Concr. Compos. 30 (2008) 290–296, https://doi.org/10.1016/j.cemconcomp.2007.05.011.
[70] G. Prokopski, B. Langier, Effect of water/cement ratio and silica fume addition on the fracture toughness and morphology of fractured surfaces of gravel concretes, Cement Concr. Res. 30 (2000) 1427–1433, https://doi.org/10.1016/S0008-8846(00)00332-X.
[71] K.L. Scrivener, K.M. Nemati, The percolation of pore space in the cement paste/aggregate interfacial zone of concrete, Cement Concr. Res. 26 (1996) 35–40, https://doi.org/10.1016/0008-8846(95)00185-9.
[72] Z. Liu, W. Hansen, Effect of hydrophobic surface treatment on freeze-thaw durability of concrete, Cem. Concr. Compos. 69 (2016) 49–60, https://doi.org/10.1016/j.cemconcomp.2016.03.001.
[73] Ministry of Infrastructure and Water Management, Soil Quality Decree (2022). https://wetten.overheid.nl/BWBR0047808/2025-05-21#BijlageA.
[74] C. Shi, A. Fernández-Jiménez, Stabilization/solidification of hazardous and radioactive wastes with alkali-activated cements, J. Hazard. Mater. 137 (2006) 1656–1663, https://doi.org/10.1016/j.jhazmat.2006.05.008.